Supporting Information

Dually Directional Glycosylated Phthalocyanines as Extracellular Red-Emitting Fluorescent Probes

Ali Husain,*[a] Asaithampi Ganesan,[a] Miloslav Machacek,[b] Lukas Cerveny,[b] Pavel Kubat,[c]Basma Ghazal,[a]Petr Zimcik,* [b] Saad Makhseed*[a]

[a]*Department of Chemistry, Kuwait University, P.O. Box 5969, Safat-13060, Kuwait.*

[b]*Faculty of Pharmacy in Hradec Kralove, Charles University, Akademika Heyrovskeho 1203, 500 05, Hradec Kralove, Czech Republic*

[c]*J. Heyrovský Institute of Physical Chemistry, v.v.i, Academy of Sciences of the Czech Republic Dolejškova 3, 182 23, Praha 8, Czech Republic*

* *Corresponding authors;* *ali.husain@ku.edu.kw*
Saad.makhseed@ku.edu.kw
zimcik@faf.cuni.cz

Table of Contents

NMR spectra

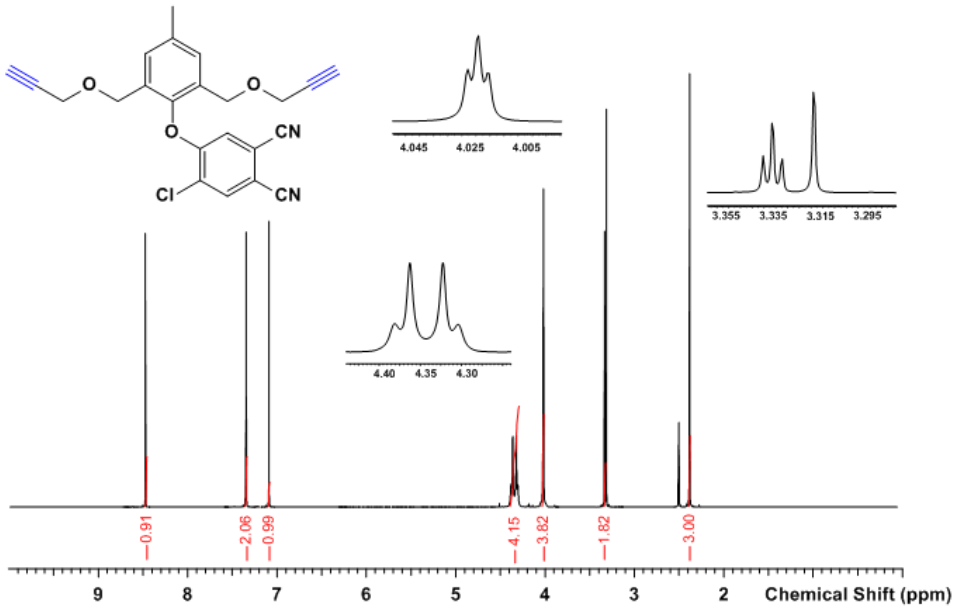

Figure S1. ^{1}H-NMR spectrum of precursor **4** in DMSO-d_6 at 25 ˚C

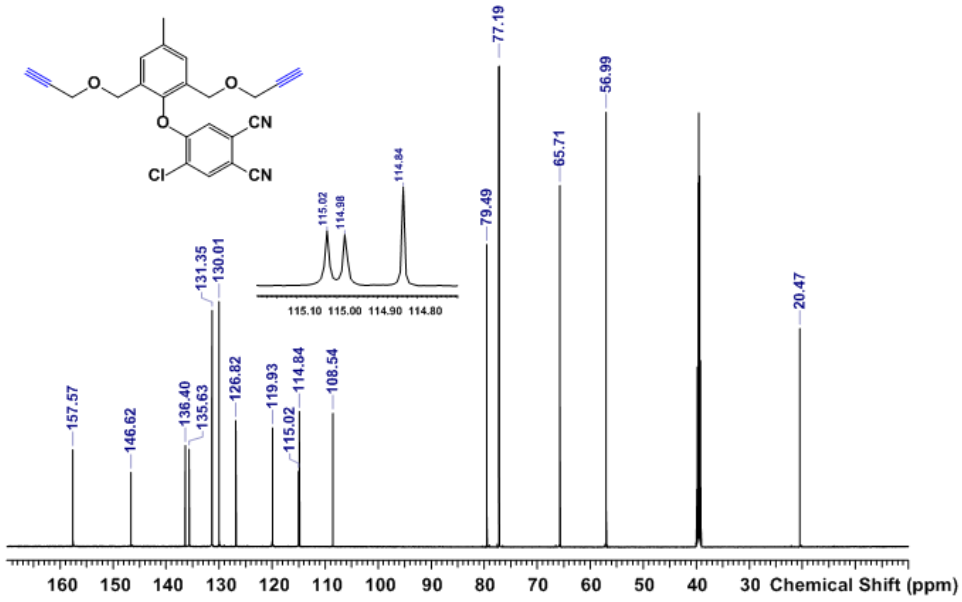

Figure S2. ^{13}C-NMR spectrum of precursor **4** in DMSO-d_6 at 25 ˚C

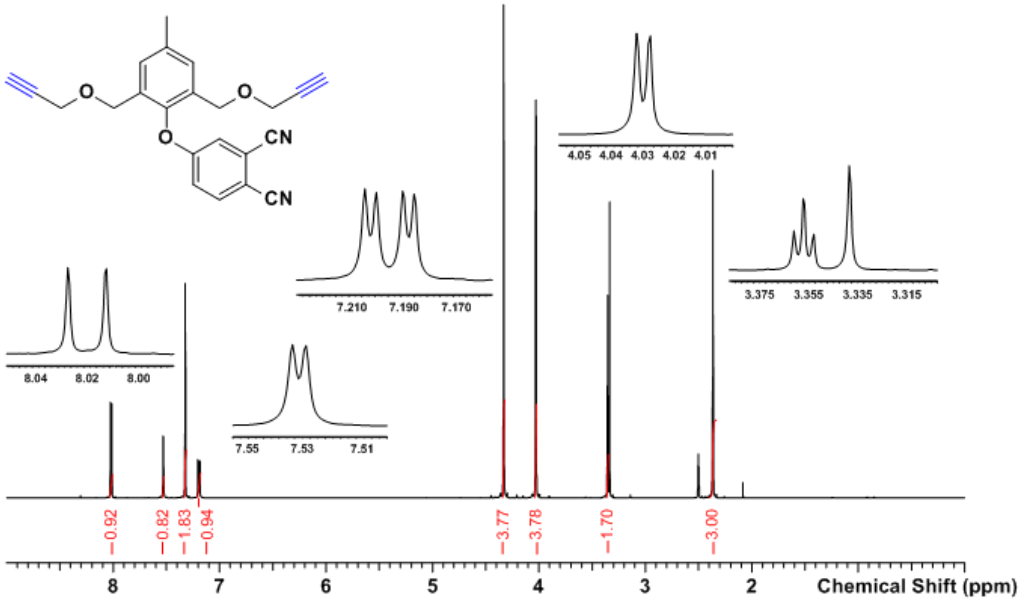

Figure S3. ^{1}H-NMR spectrum of precursor **5** in DMSO-d_6 at 25 ˚C

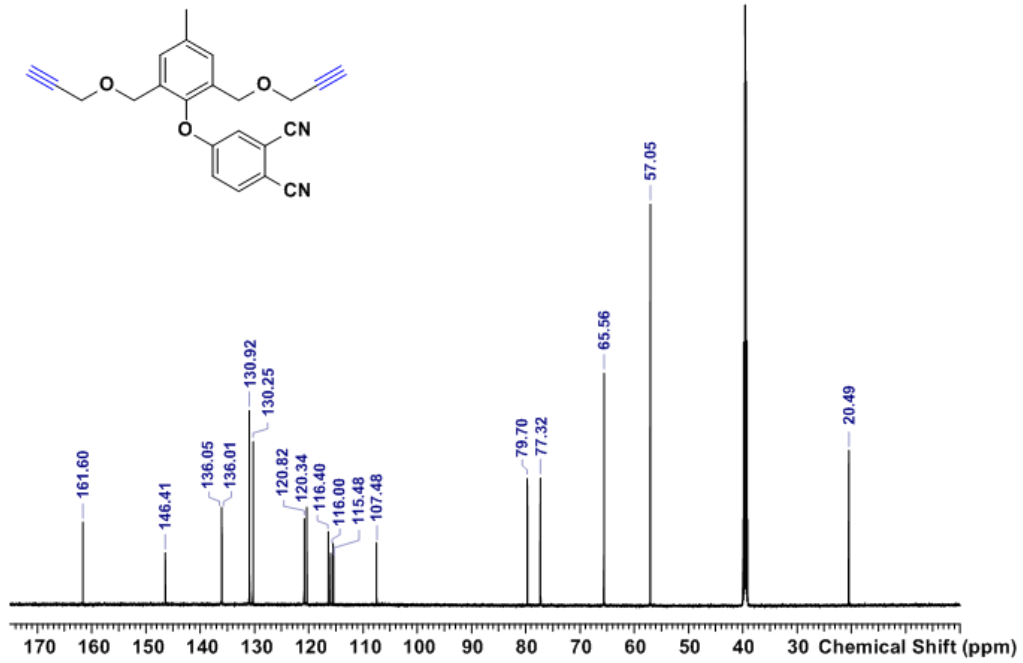

Figure S4. ^{13}C-NMR spectrum of precursor **5** in DMSO-d_6 at 25 ˚C

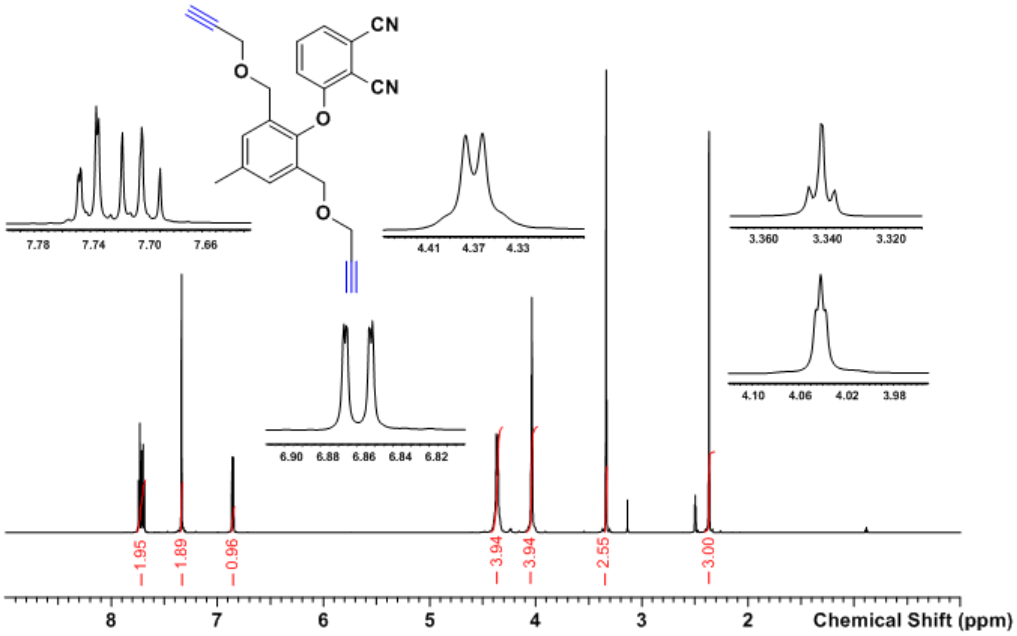

Figure S5. ^{1}H-NMR spectrum of precursor **6** in DMSO-d_6 at 25 ˚C

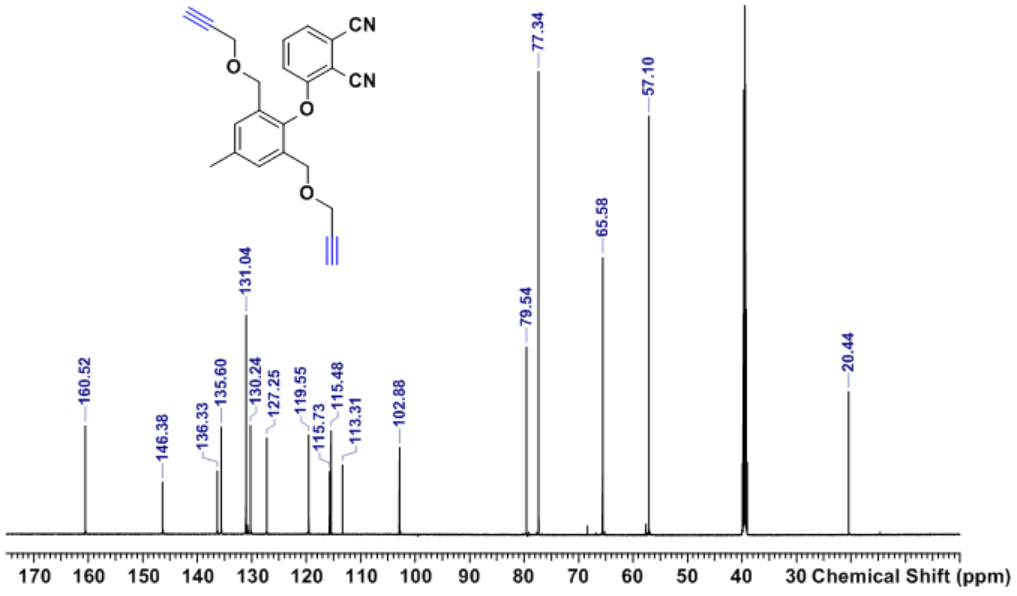

Figure S6. ^{13}C-NMR spectrum of precursor **6** in DMSO-d_6 at 25 ˚C.

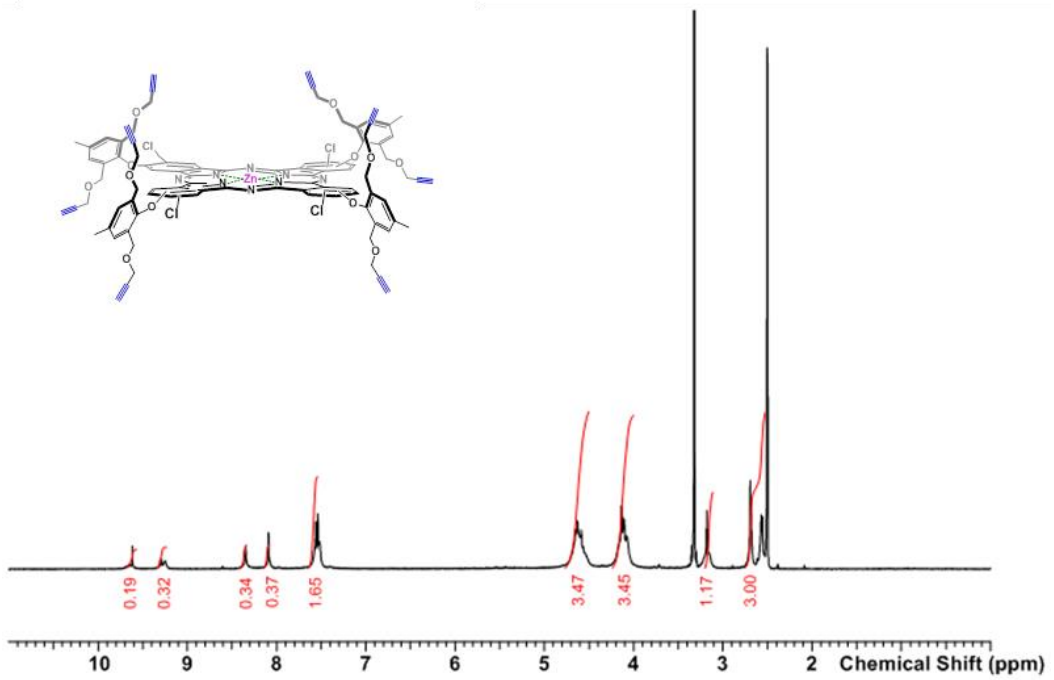

Figure S7. ^{1}H-NMR spectrum of **Pc2** in DMSO-d_6 at 25 ˚C

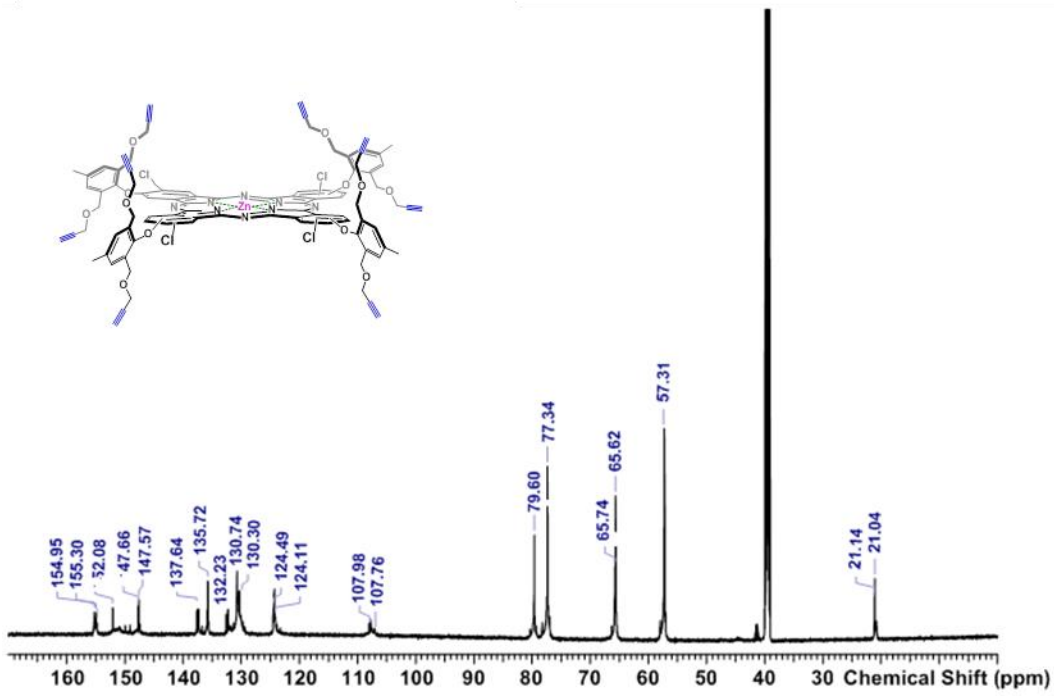

Figure S8. ^{13}C-NMR spectrum of **Pc2** in DMSO-d_6 at 25 ˚C

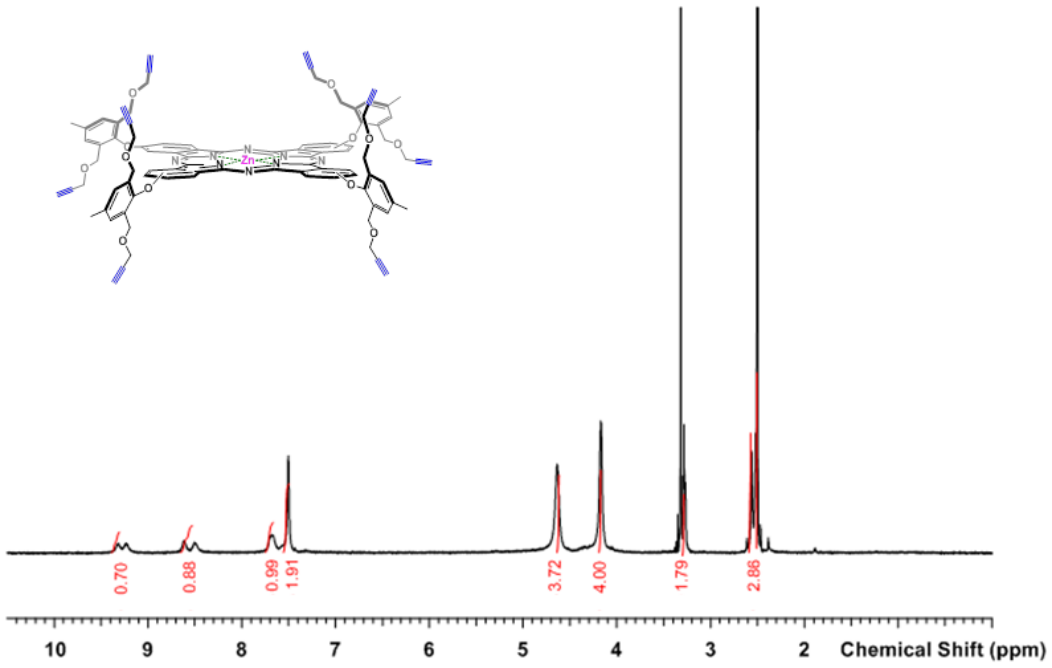

Figure S9. ^{1}H-NMR spectrum of **Pc3** in DMSO-d_6 at 25 ˚C

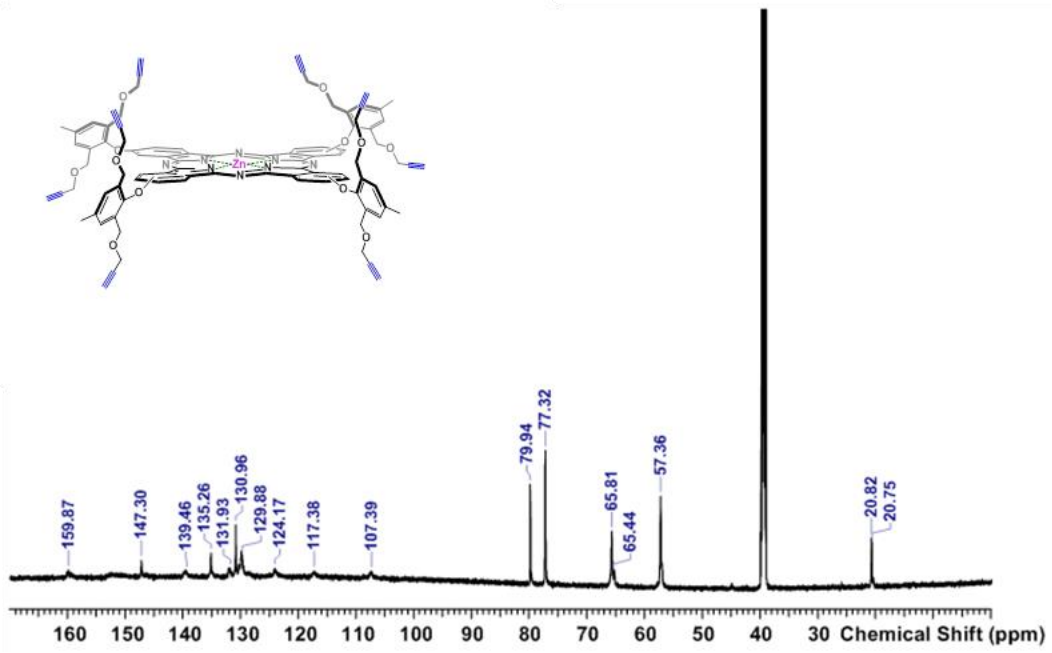

Figure S10. ^{13}C-NMR spectrum of **Pc3** in DMSO-d_6 at 25 ˚C

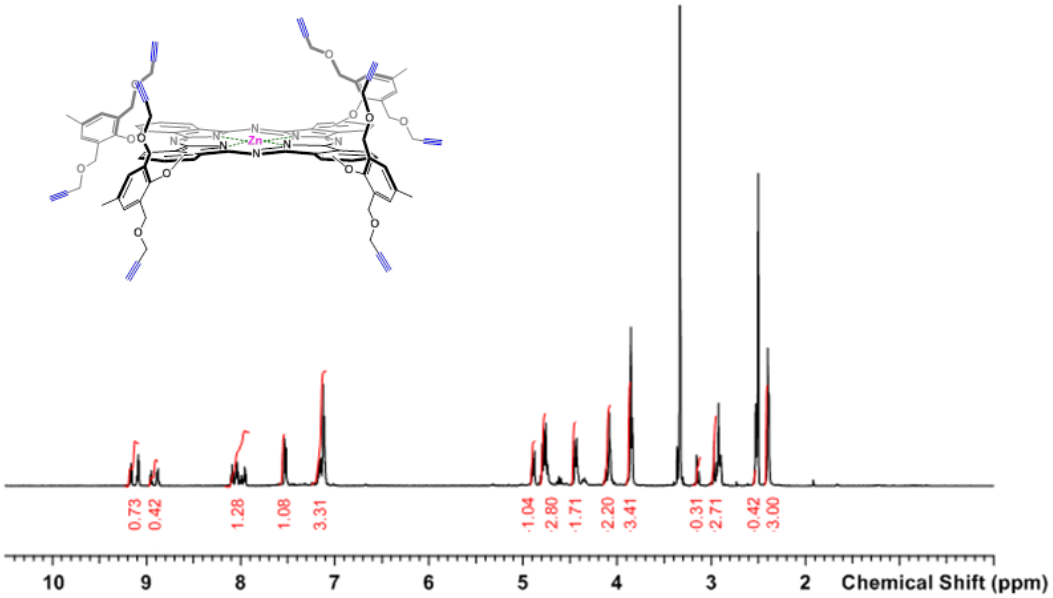

Figure S11.[1]H-NMR spectrum of **Pc4** in DMSO-d_6 at 25 ˚C.

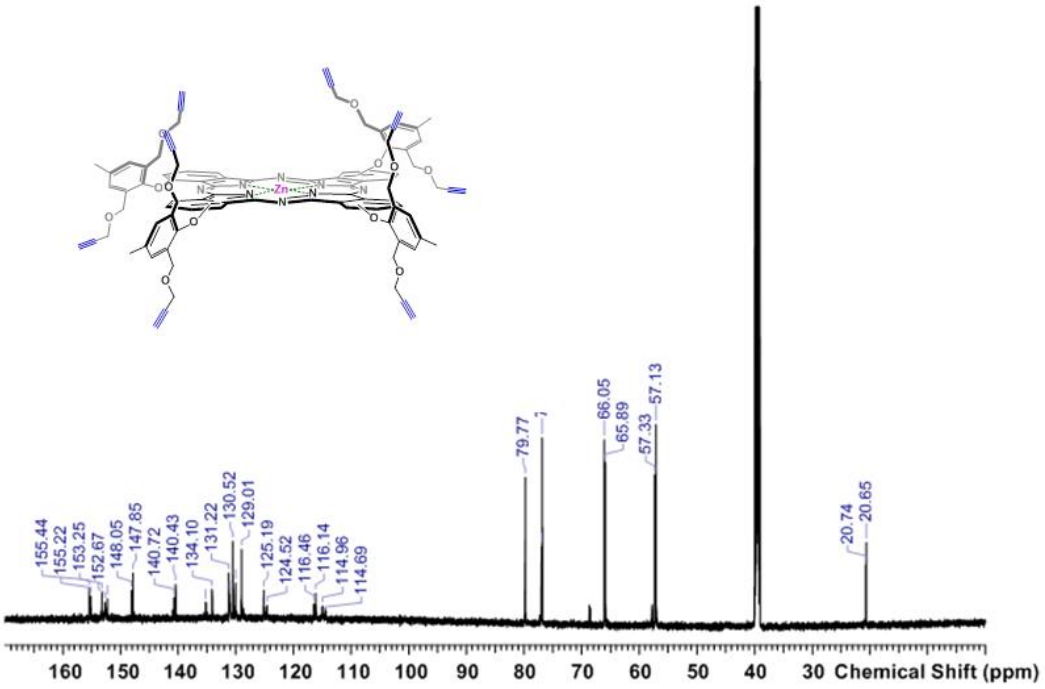

Figure S12.[13]C-NMR spectrum of **Pc4** in DMSO-d_6 at 25 °C

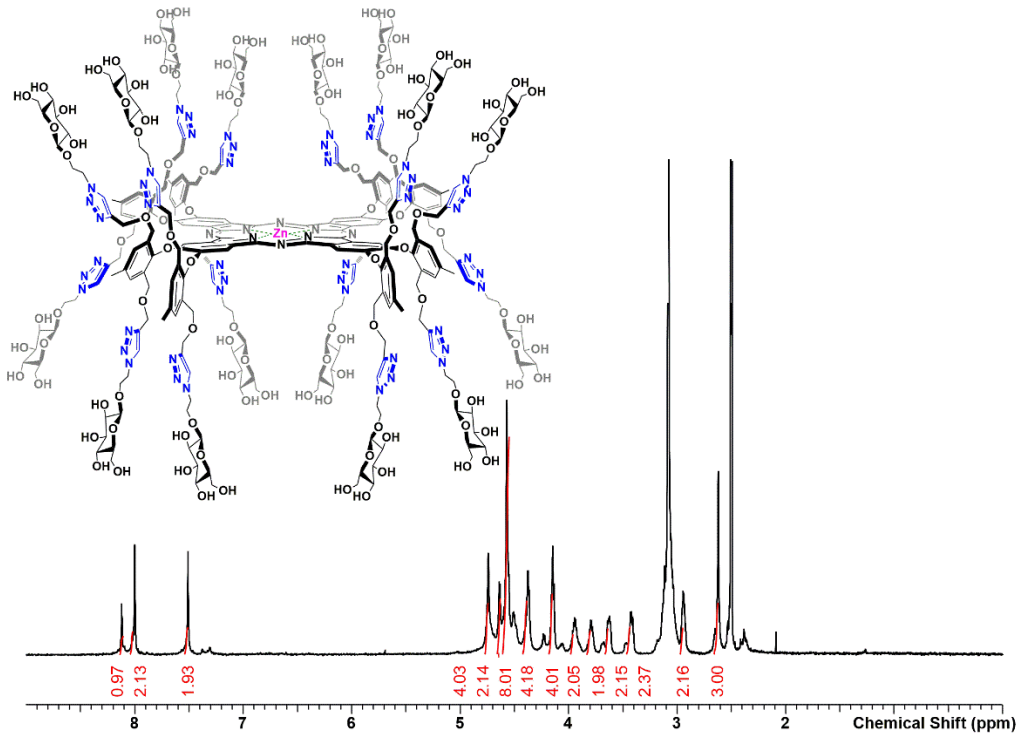

Figure S13. ^{1}H-NMR spectrum of **PcG1** in DMSO-d_6 at 95 ˚C

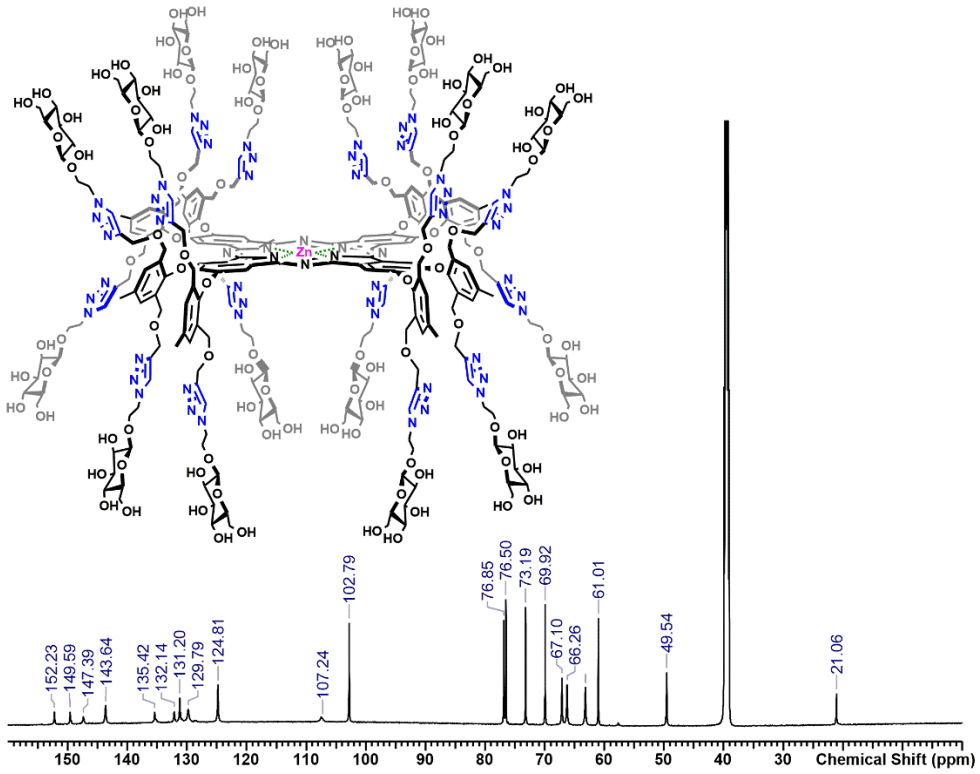

Figure S14. ^{13}C-NMR spectrum of **PcG1** in DMSO-d_6 at 25 ˚C

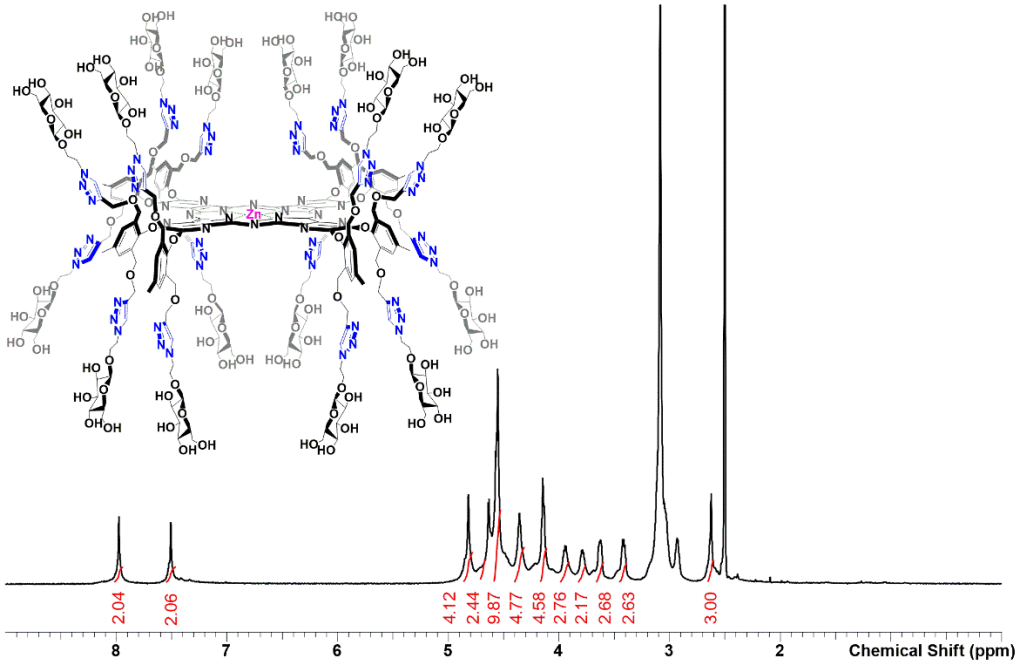

Figure S15. ^{1}H-NMR spectrum of **AzaPcG1** in DMSO-d_6 at 95 °C

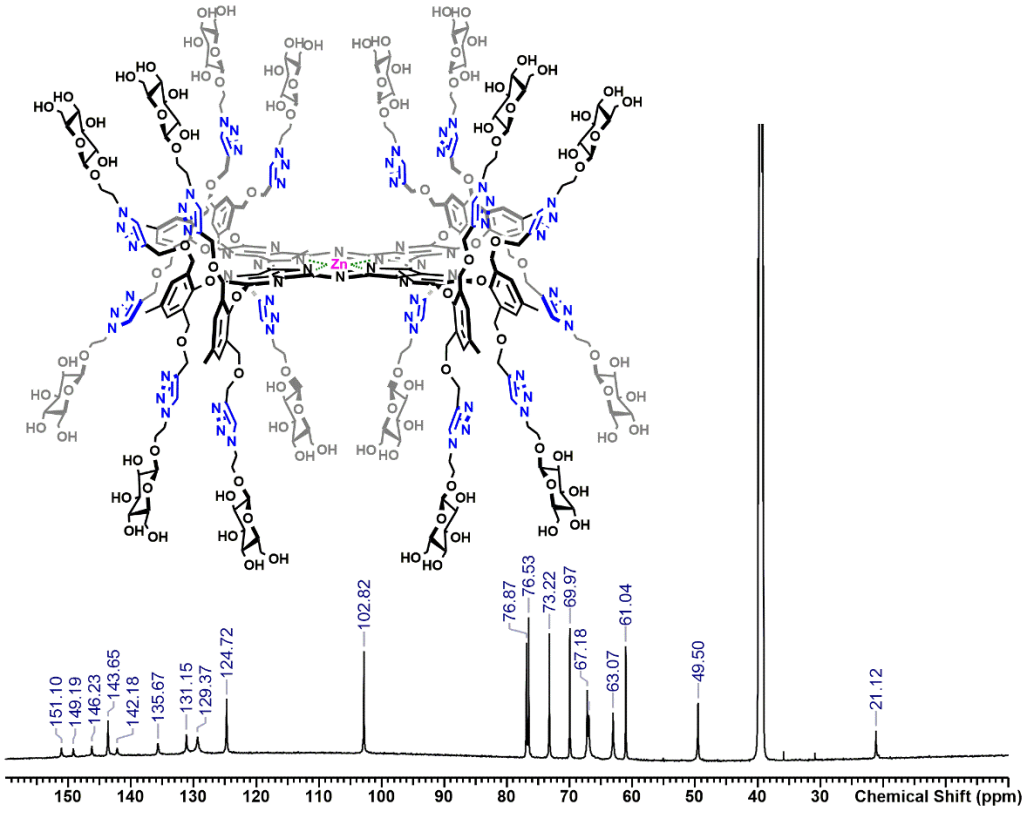

Figure S16. ^{13}C-NMR spectrum of **AzaPcG1** in DMSO-d_6 at 25 ˚C

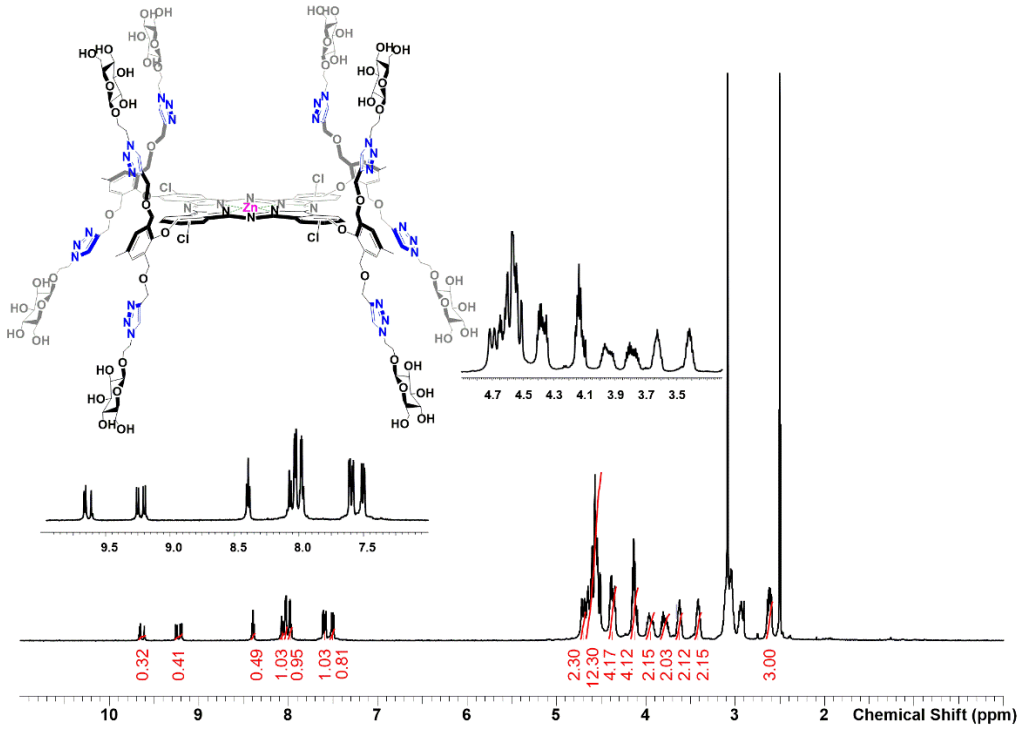

Figure S17. ^{1}H-NMR spectrum of **PcG2** in DMSO-d_6 at 95 ˚C

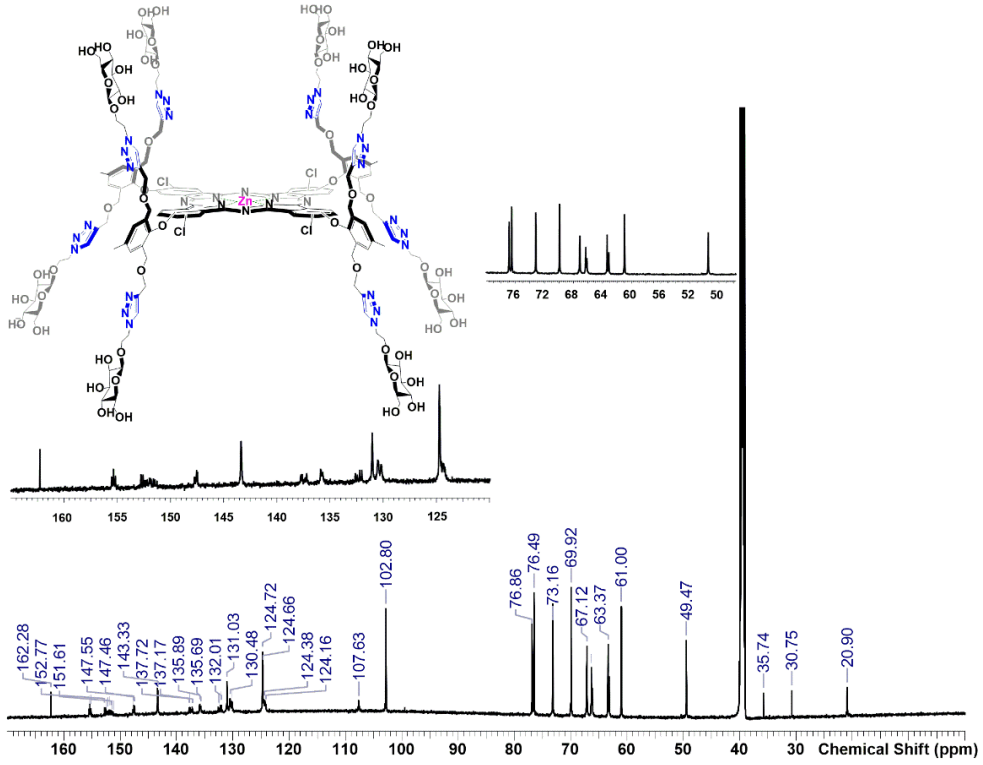

Figure S18. ^{13}C-NMR spectrum of **PcG2** in DMSO-d_6 at 25 ˚C

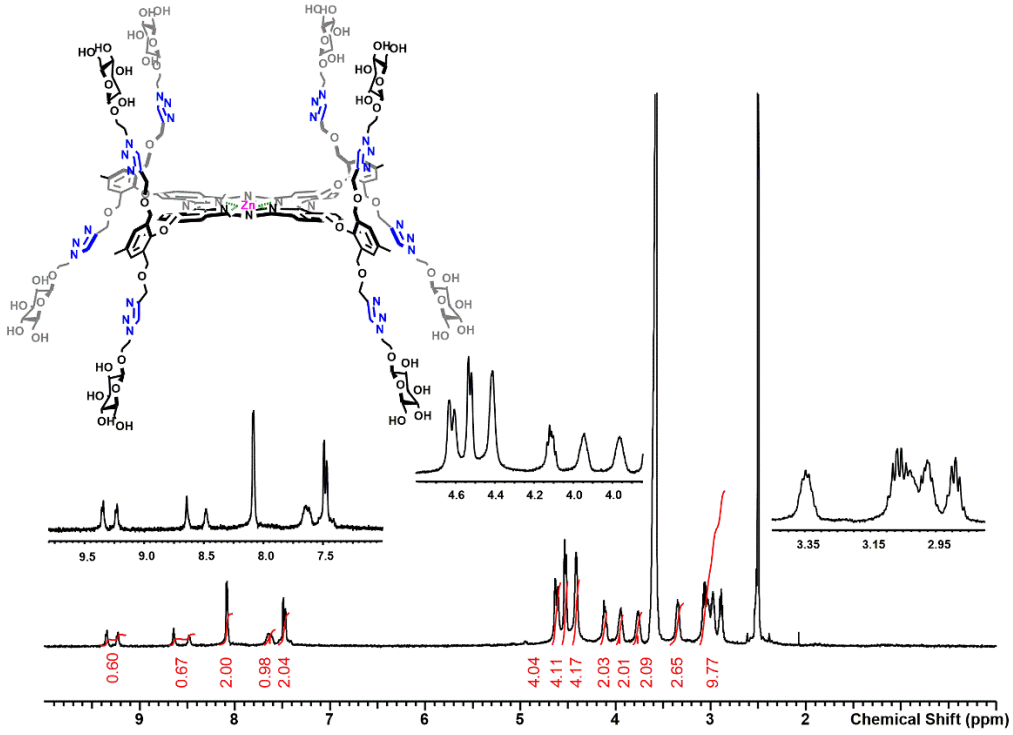

Figure S19. ^{1}H-NMR spectrum of **PcG3** in DMSO-d_6 at 95 ˚C

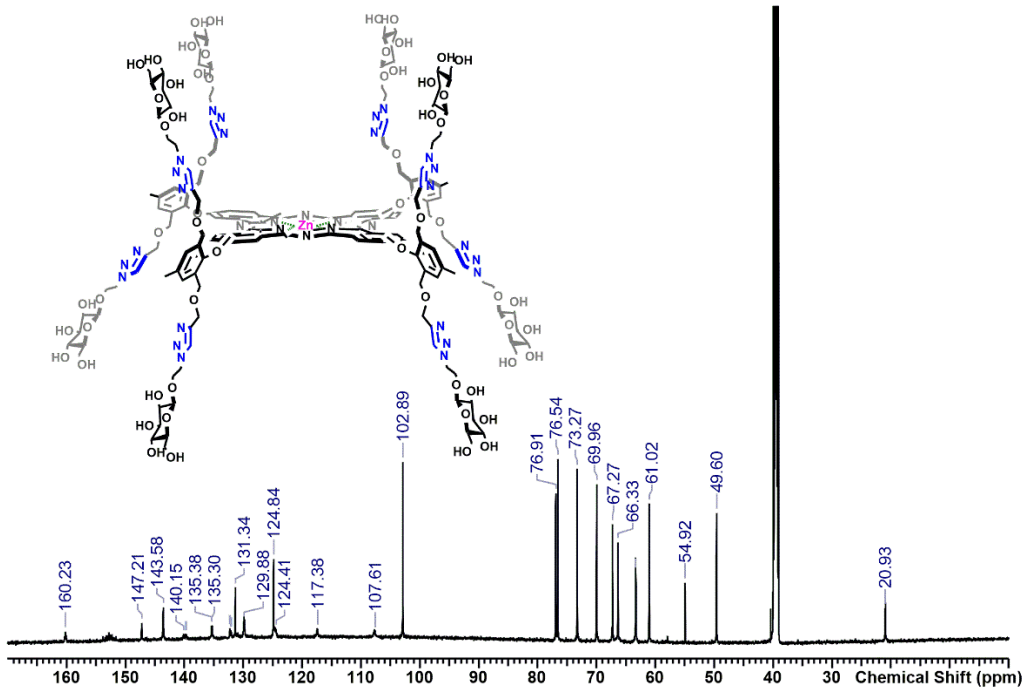

Figure S20. ^{13}C-NMR spectrum of **PcG3** in DMSO-d_6 at 25 ˚C

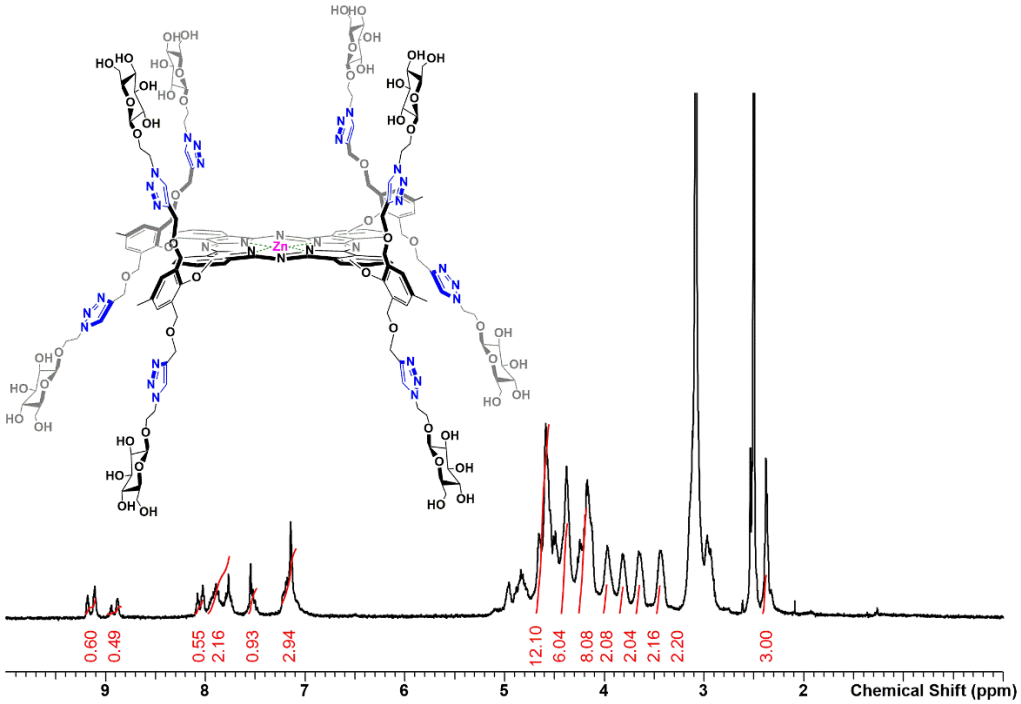

Figure S21. ^{1}H-NMR spectrum of **PcG4**in DMSO-d_6 at 95 ˚C

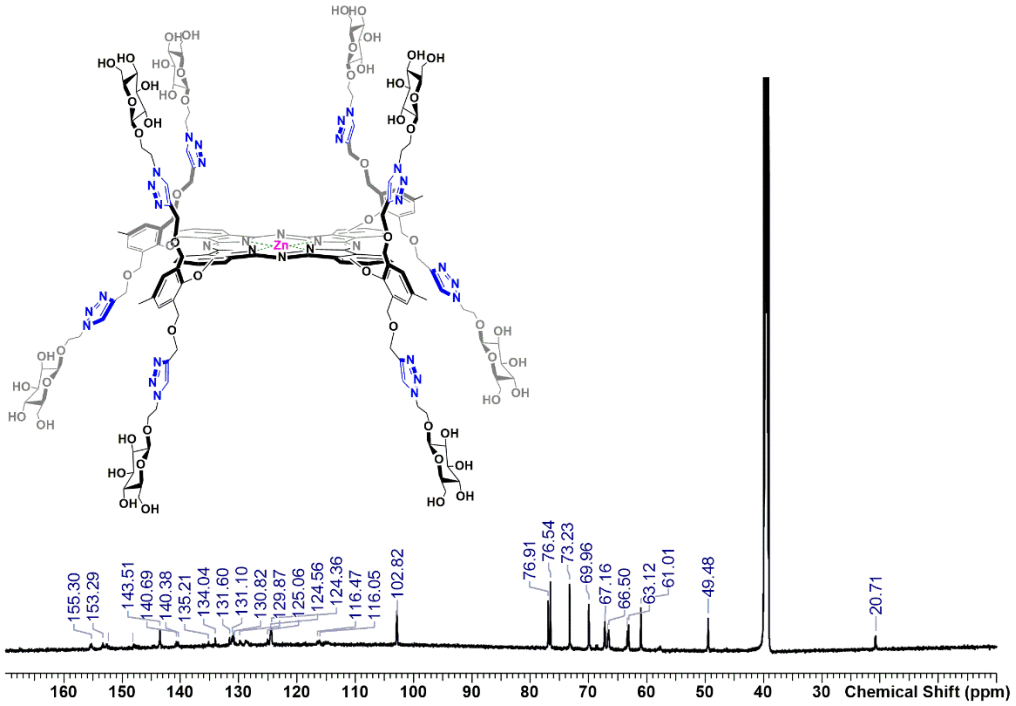

Figure S22. ^{13}C-NMR spectrum of **PcG4** in DMSO-d_6 at 25 ˚C

Mass Spectra

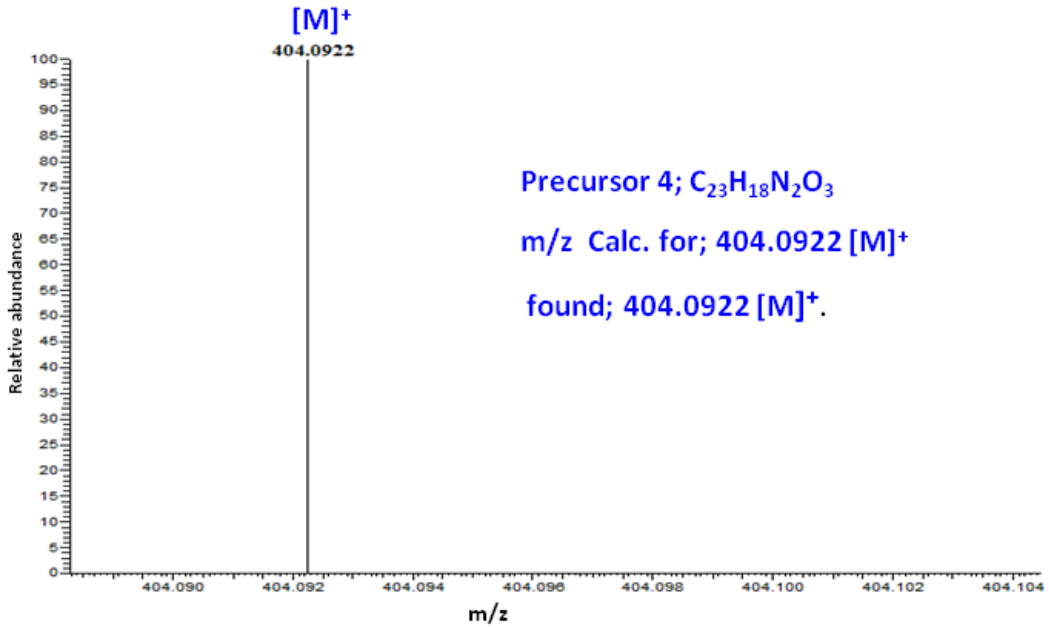

Figure S23. HRMS spectrum of Precursor **4**

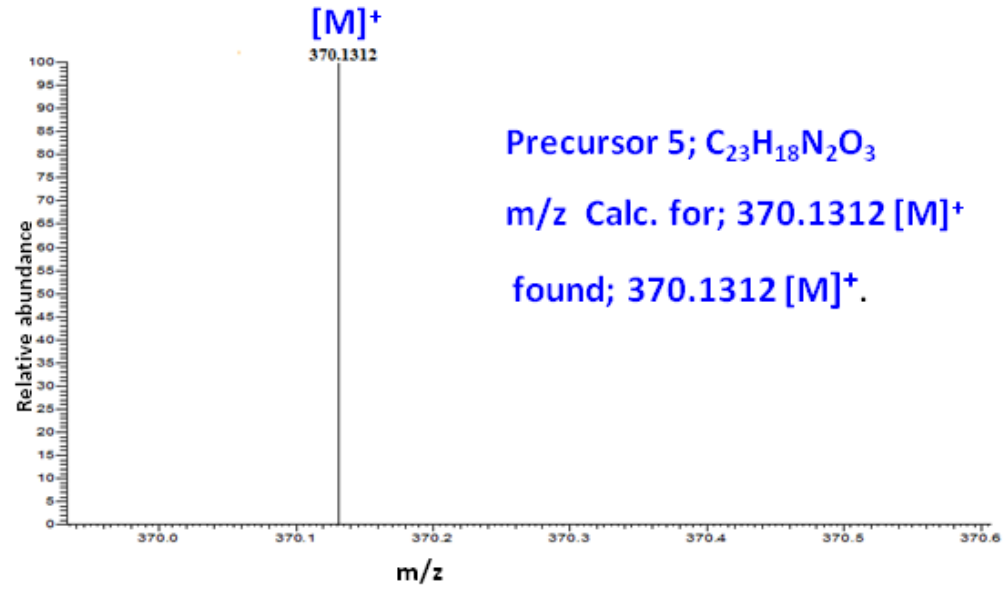

Figure S24. HRMS spectrum of Precursor **5**

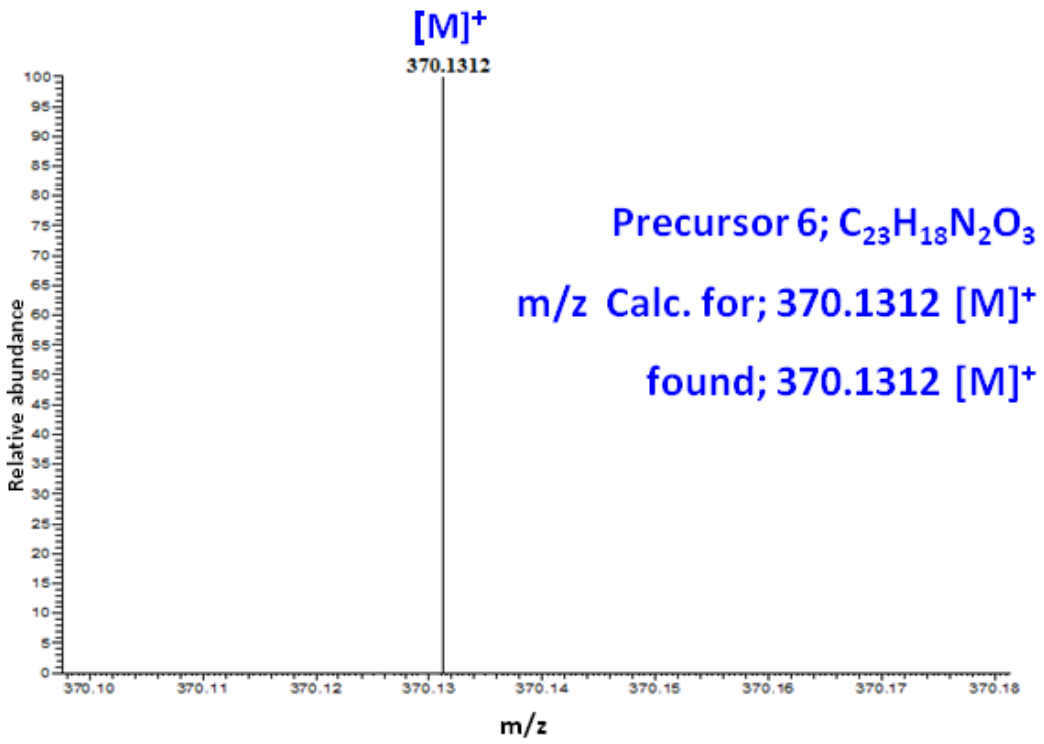

Figure S25. HRMS spectrum of Precursor **6**

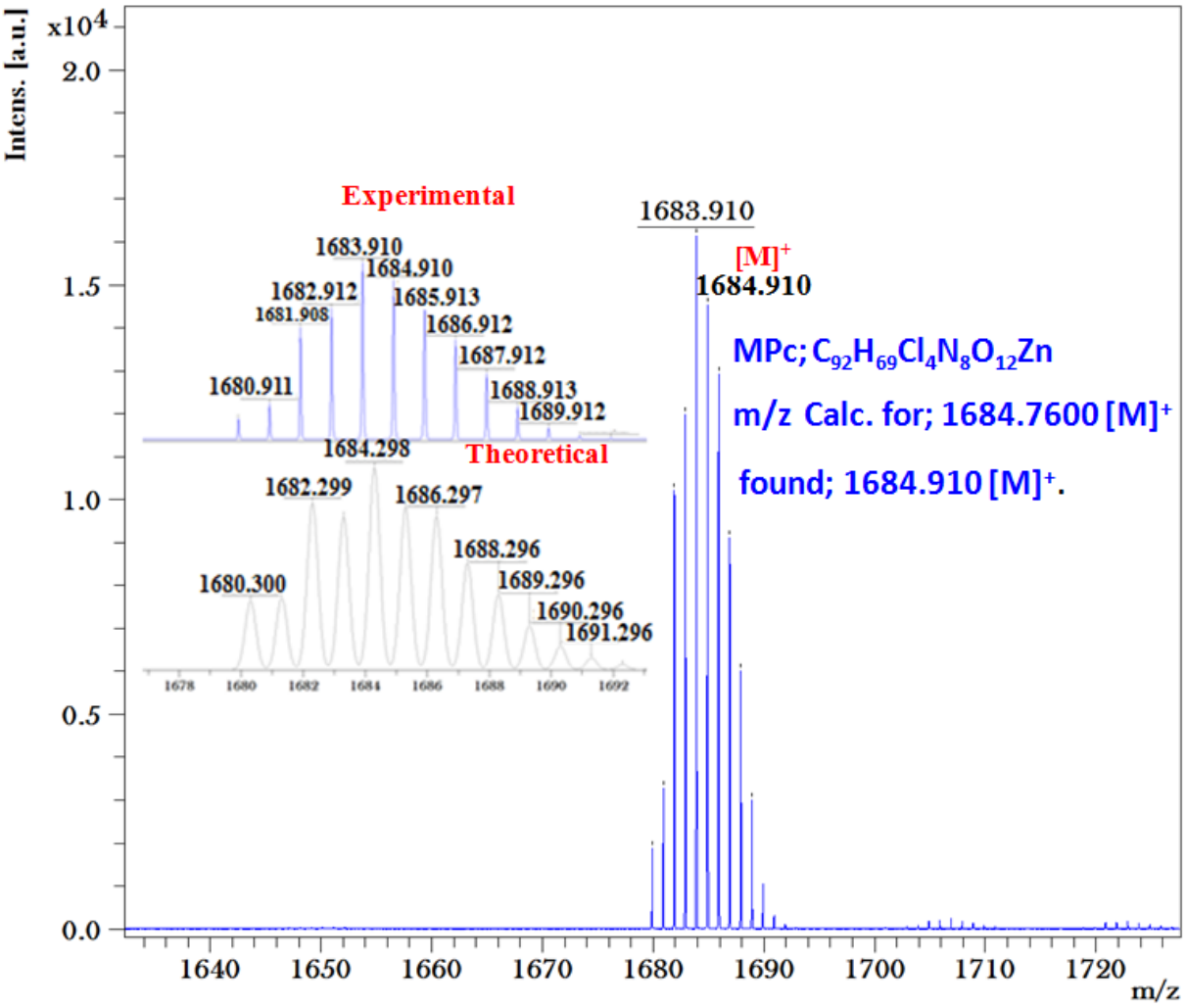

Figure S26. MALDI-MS spectrum of **Pc2**

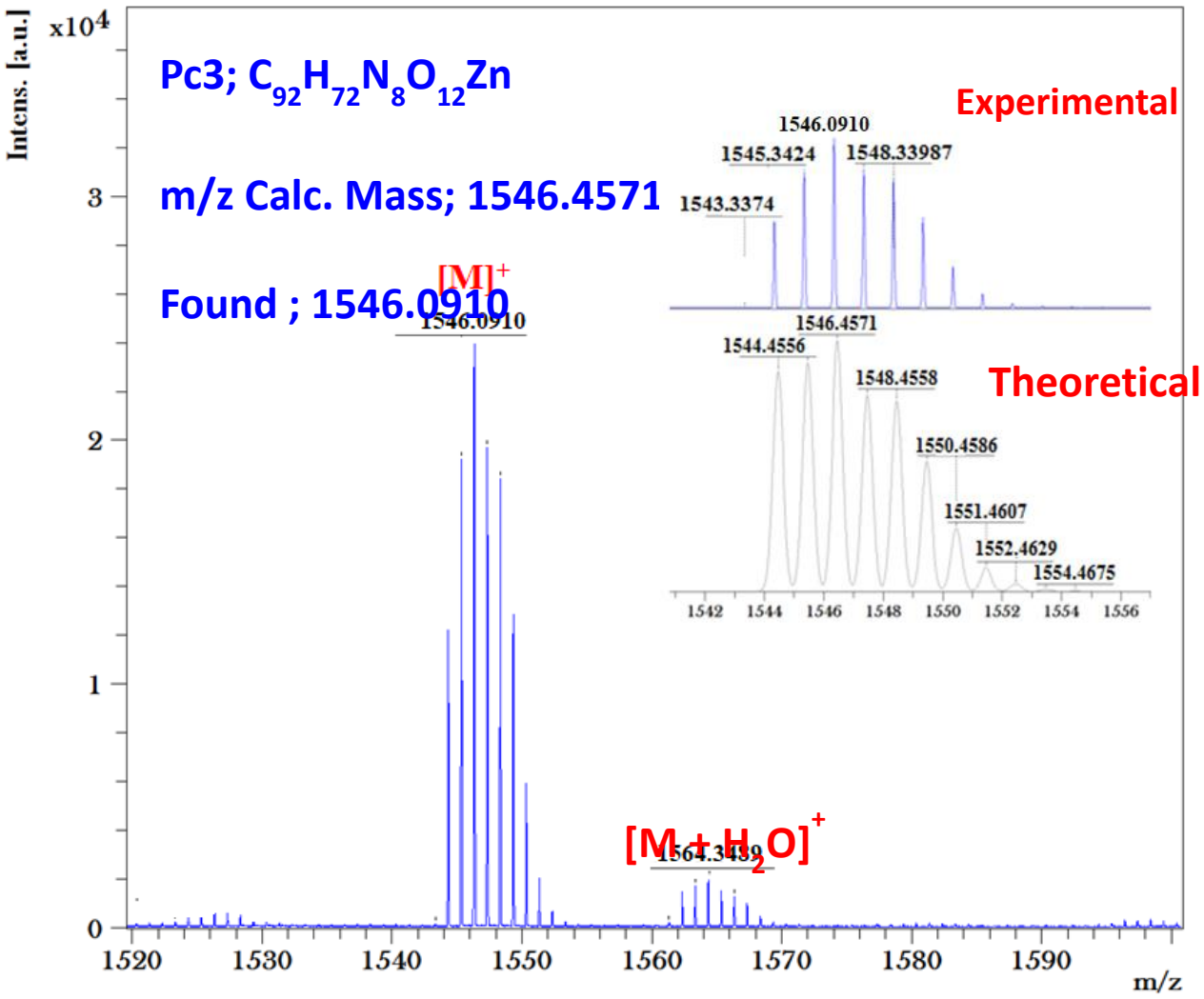

Figure S27. MALDI-MS spectrum of **Pc3**

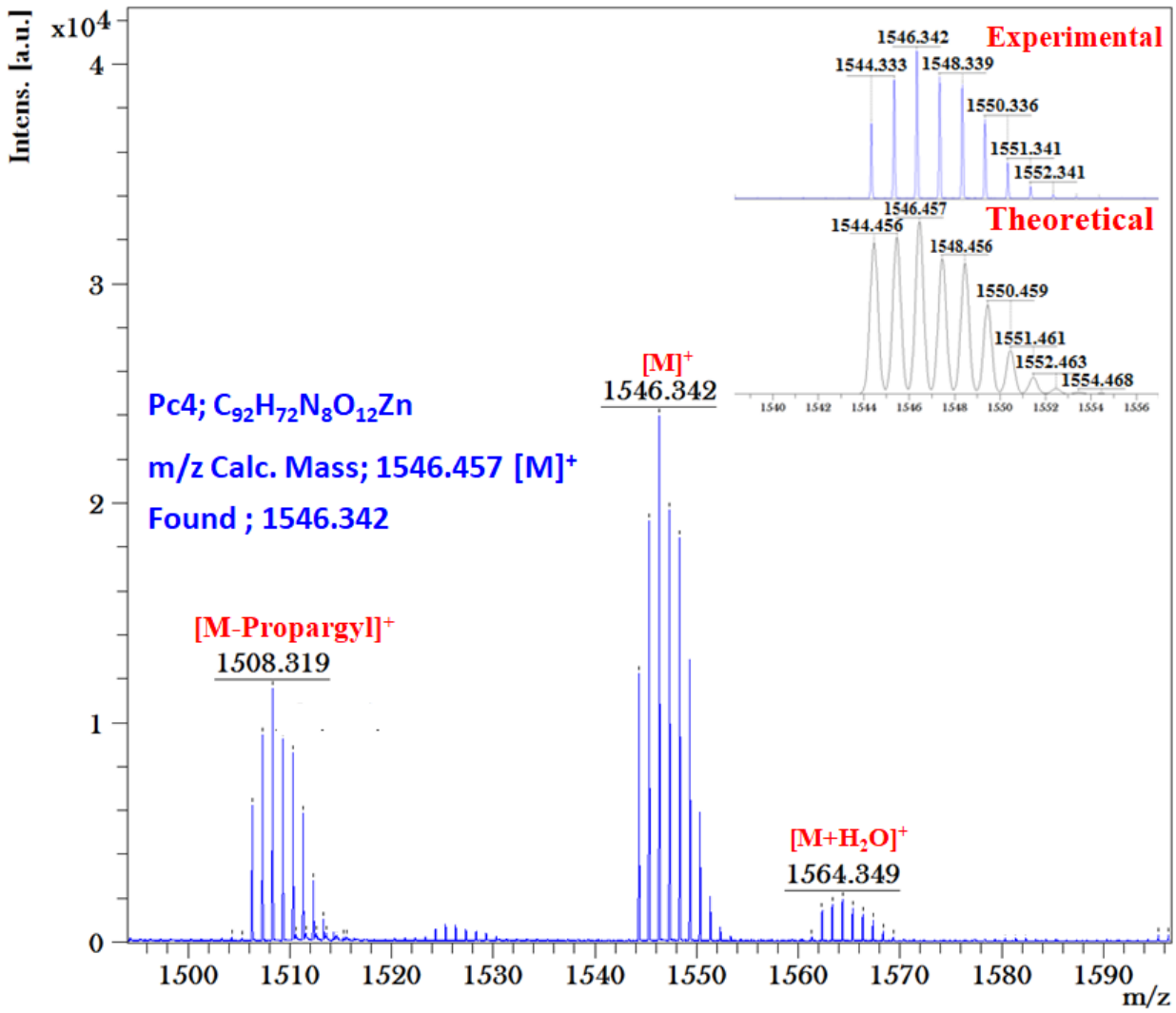

Figure S28. MALDI-MS spectrum of **Pc4**

FT-IR Spectra

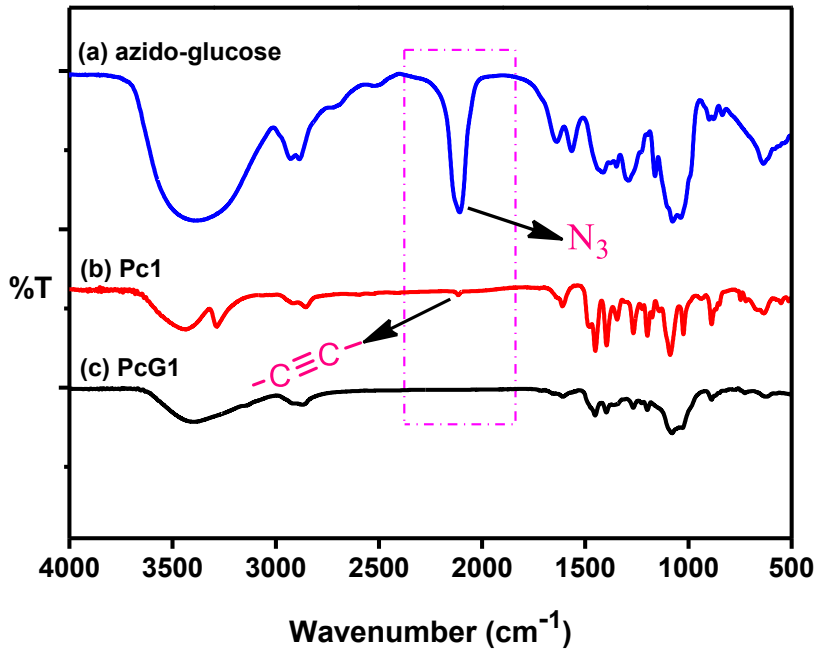

Figure S29. FT-IR spectra of (a) **azido-glucose** derivative;(b) **Pc1** and (c) **PcG1**

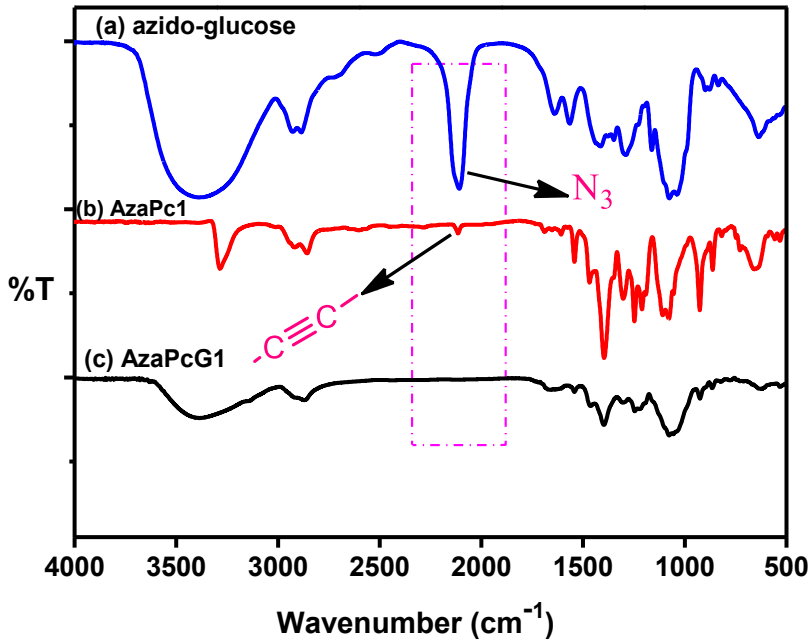

Figure S30. FT-IR spectra of (a) **azido-glucose** derivative;(b) **AzaPc1** and (c) **AzaPcG1**

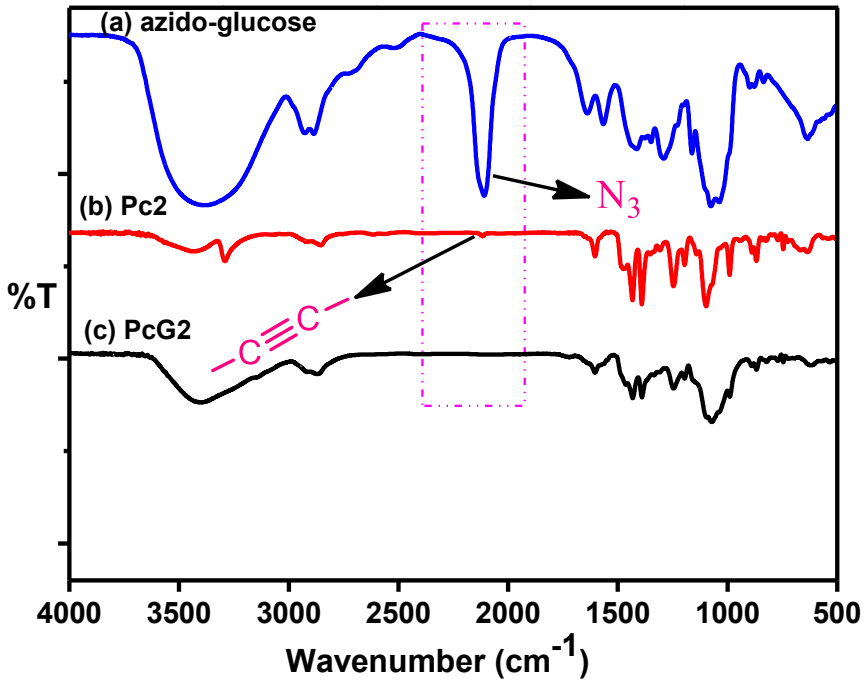

Figure S31. FT-IR spectra of (a) **azido-glucose** derivative;(b) **Pc2** and (c) **PcG2**

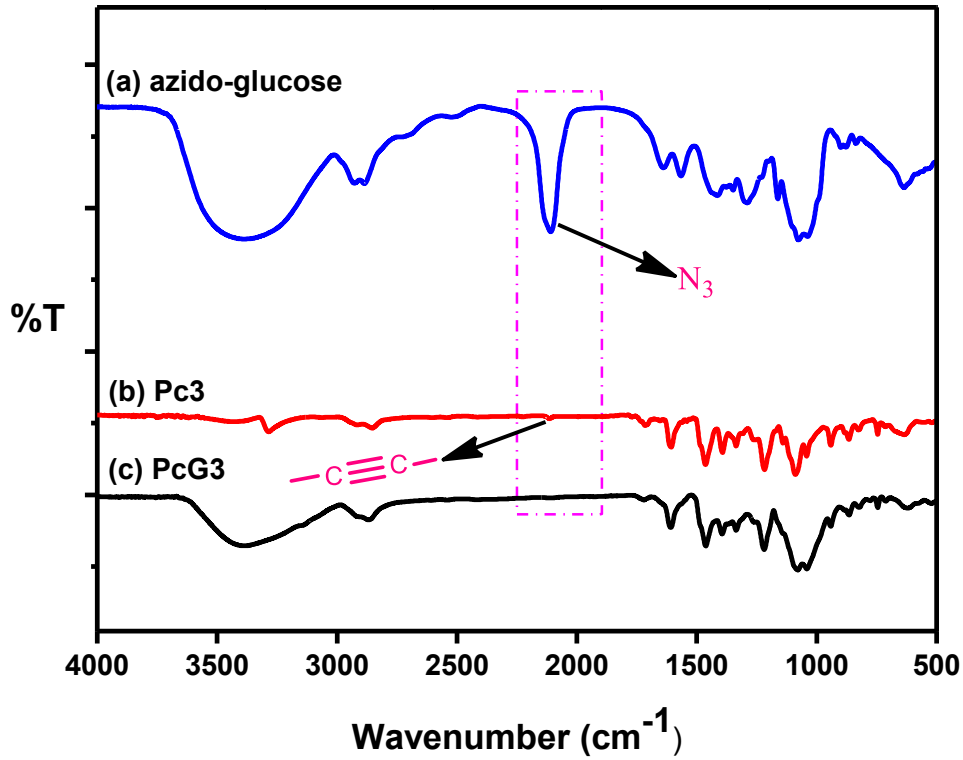

Figure S32. FT-IR spectra of (a) **azido-glucose** derivative;(b) **Pc3** and (c) **PcG3**

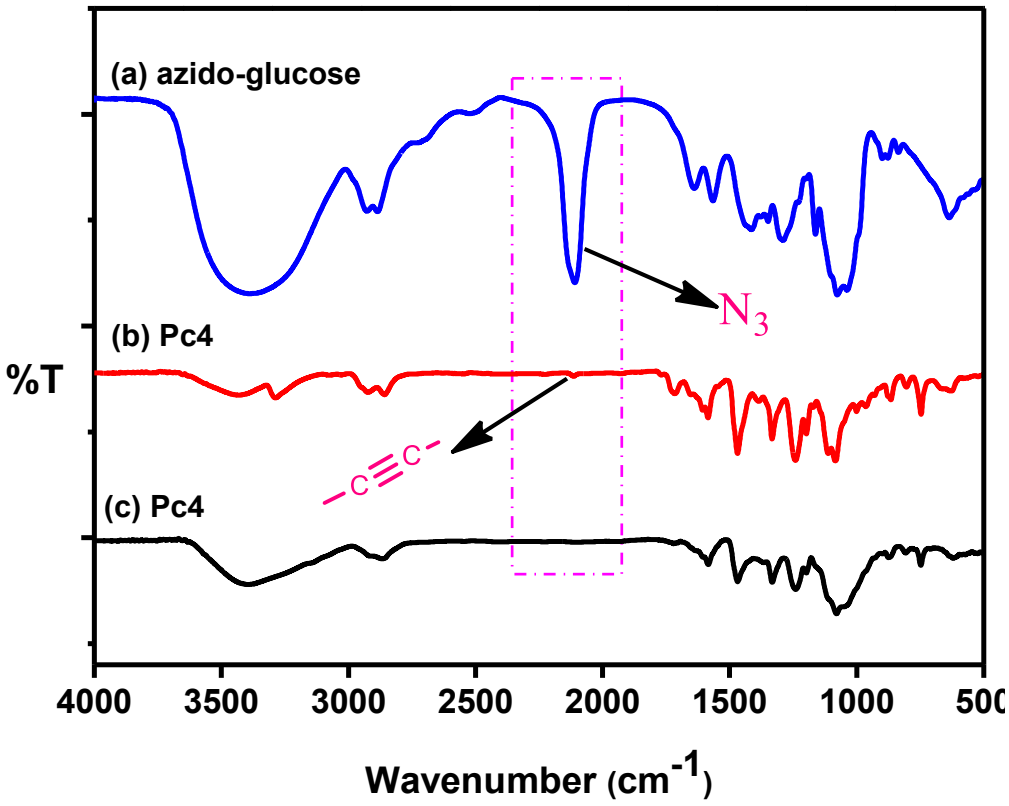

Figure S33. FT-IR spectra of (a) **azido-glucose** derivative;(b) **Pc4** and (c) **PcG4**

Ultra-High-performance liquid chromatography (UHPLC)

The purity of all glycosylated macrocycles (**PcG1-G4**, **AzaPcG1**) was determined by using UHPLC system consists of LC Shimadzu Nexera X2 with an SPD 20A UV detector with a sensitivity of 0.5 × 10^{-5} AU and a linearity of 2.5 AU (wavelength range 190-800nm).The chromatographic conditions have been studied in order to obtain an appropriate adequacy of the system. The mobile phase composition was tested with water / acetonitrile (10:90 v / v) using a Thermo Hypersil Gold C18 column (100 × 2.1 mm × 5 µm). Routine degassing of the mobile phase was performed by passing it through a 0.2 µm (47 mm) GHP membrane filter (Pall Corporation, Michigan). The mobile phase was pumped isocratically at a flow rate of 0.5 ml / min at 25 °C and the sample injection volume of 10 µL as well. All the samples were dissolved in water/acetonitrile (1:1 v/v) followed by sonication and subjected to analysis. HPLC results of all the glycol macrocycles are shown in Table **S1** and Figures **S34-38**. All the synthesized macrocycles displayed well resolved single peak at chromatogram and they showed >**99.999%** purity.

Table S1: UHPLC for the symmetrical glycomacrocycles (**PcG1/AzaPcG1**) and the structural isomers glycomacrocycles (**PcG2-PcG4**)

Sample name	Retention time	λ_{max}	Area%
PcG1	1.450	680nm	100
AzaPcG1	1.454	630nm	100
PcG2	1.410	680nm	100
PcG3	1.484	680nm	100
PcG4	1.269	700nm	100

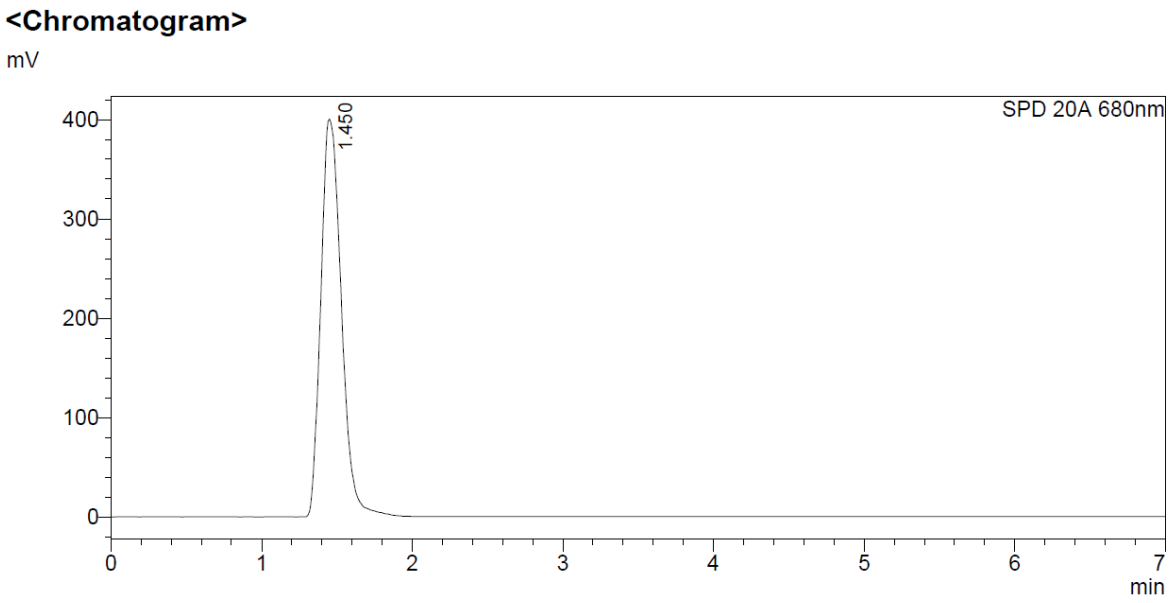

Peak Table

SPD 20A 680nm

Peak#	Ret. Time	Area	Area%
1	1.450	3871524	100.000
Total		3871524	100.000

Figure S34. HPLC purity analysis for **PcG1**

<Chromatogram>

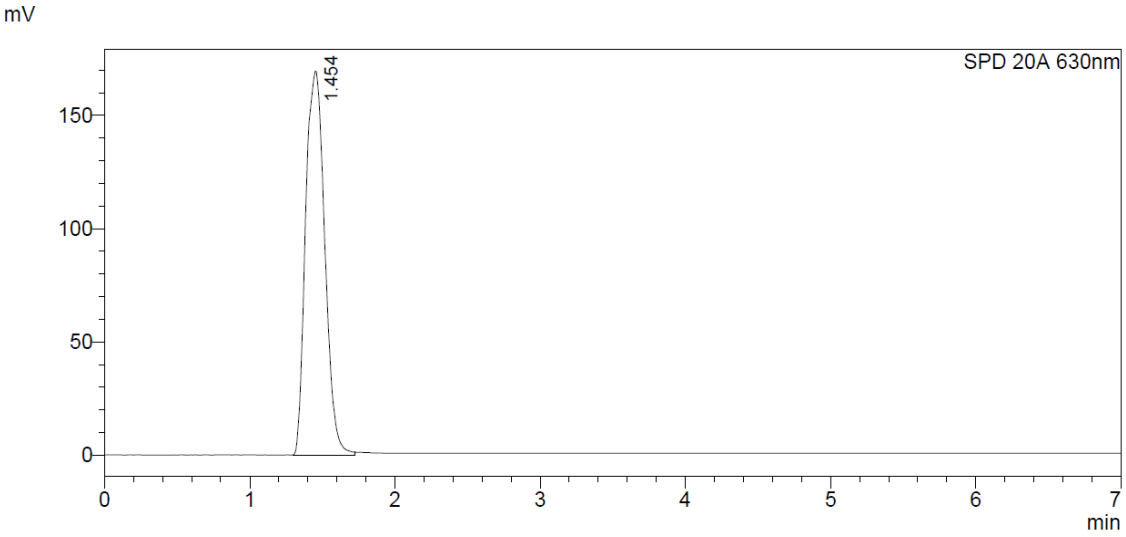

Peak Table

SPD 20A 630nm

Peak#	Ret. Time	Area	Area%
1	1.454	1555697	100.000
Total		1555697	100.000

Figure S35. HPLC purity analysis for **AzaPcG1**

<Chromatogram>

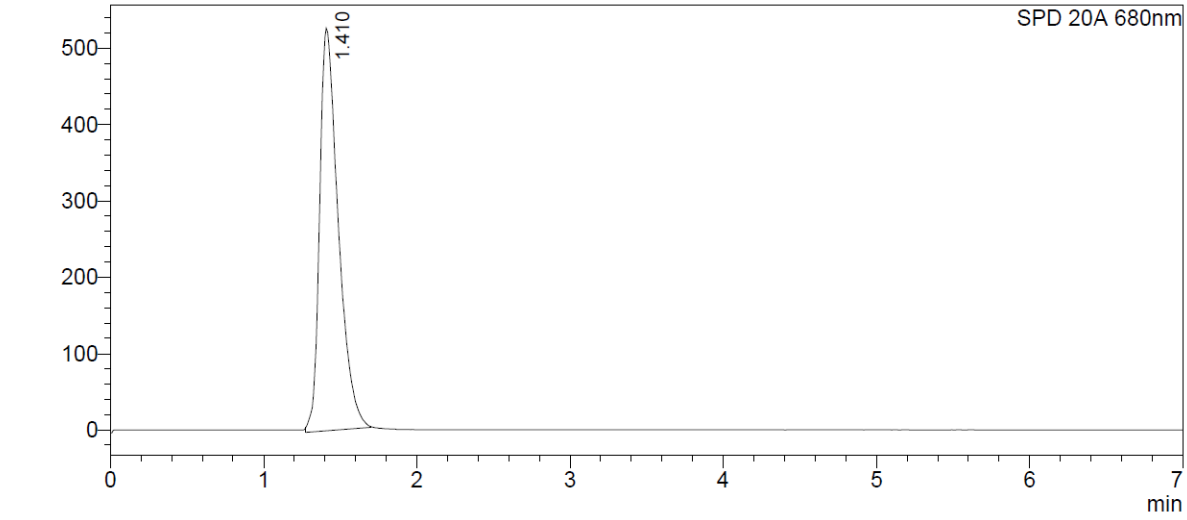

Peak Table

SPD 20A 680nm

Peak#	Ret. Time	Area	Height	Area%
1	1.410	4466624	527198	100.000
Total		4466624	527198	100.000

Figure S36. HPLC purity analysis for **PcG2**

<Chromatogram>

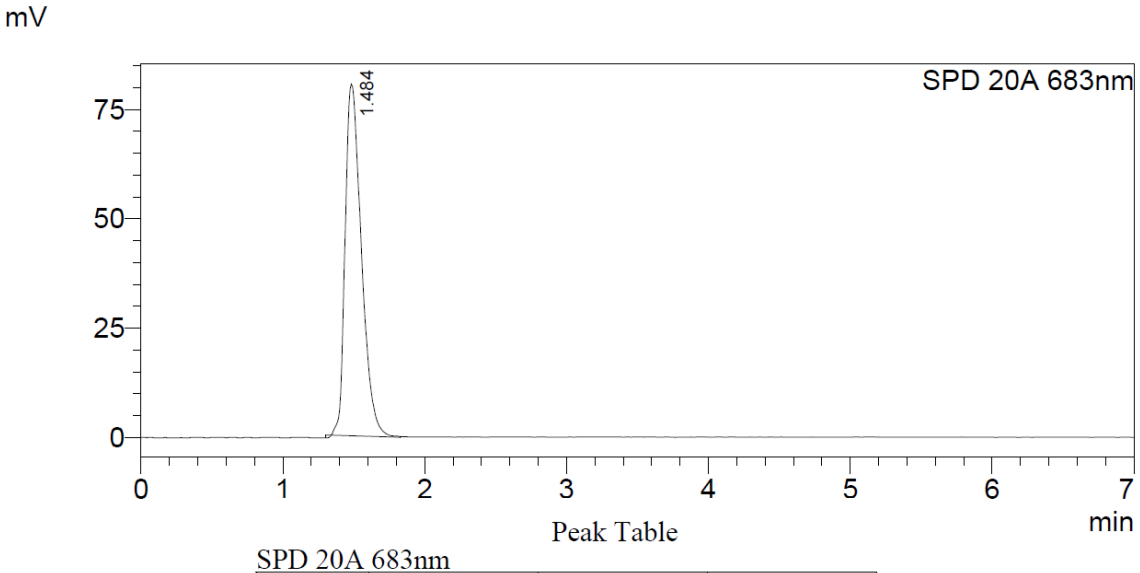

Peak Table

SPD 20A 683nm

Peak#	Ret. Time	Area	Area%
1	1.484	641604	100.000
Total		641604	100.000

Figure S37. HPLC purity analysis for **PcG3**

<Chromatogram>

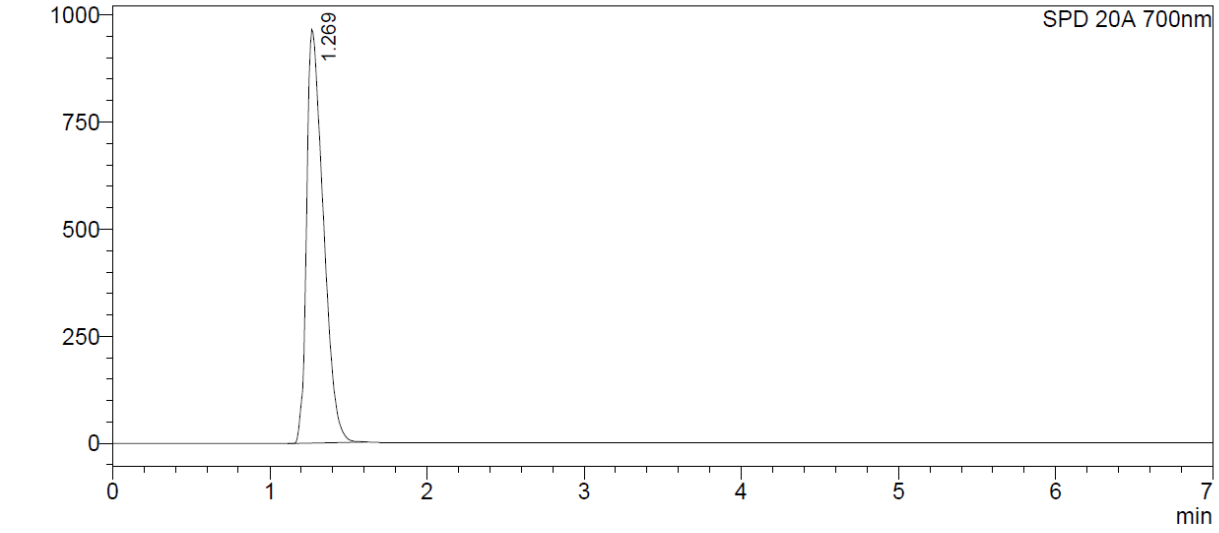

Peak Table

SPD 20A 700nm

Peak#	Ret. Time	Area	Area%
1	1.269	7156048	100.000
Total		7156048	100.000

Figure S38. HPLC purity analysis for **PcG4**

Single crystal X-ray diffraction

Experimental

The single crystal data collections were made either on Rigaku R-AXIS RAPID II diffractometer by filtered Mo-Kα radiation or using Bruker X8 Prospector employing Cu-Kα radiation. In the former case 'Crystal clear' software package was employed to generate hkl and p4p files. The structures were then solved by direct methods using crystal structure crystallographic software package except for refinement, which was performed using SHELXL-97 or SHELXL-2017/1. The reflection frames obtained from Bruker diffractometer were integrated with SAINT Software package using a narrow-frame algorithm. Finally, the structure was solved and refined using the Bruker SHELXTL Software Package. The data was collected either at room temperature or under liquid nitrogen (Oxford cryo systems).

Discussion

Crystal structures of propargyl functionalized Pc-precursors (4-6)

Pyrazine and phthalonitrile precursors having mono-substituted phenoxyl groups with terminal alkyne units were analyzed by single crystal X-ray diffraction technique. These phenoxyl groups are either at the peripheral position with respect to the phtalonitrile plane (**4**, **5**) or at the non-peripheral position (**6**). In compound **4**, there is additional chlorine which is substituted at the second peripheral position. The crystal structure of all these precursors provides valuable information regarding the orientation of phenoxyl units and terminal alkyne units with respect to the phthalonitrile plane.

The structures of phthalonitrile substrates with propargyl moieties, which are obtained from single crystal diffraction analysis, are depicted in Figures **S39**and their corresponding crystallographic parameters are given inTable **S2**. The plane of the phenoxyl ring having the alkynyl ends are oriented almost perpendicular to the plane of the phenyl rings containing the nitrile groups (the corresponding torsion angles are presented in Table **S3**). This is due to the restricted rotation imposed on phenoxyl moieties by the alkyne substituents which are presented at the *ortho* positions of the phenyl groups. Such a blocked rotation caused by the propargyl chains is enough for ensuring the non-aggregating feature for those Pc systems which are prepared from these unique molecules by the metal mediated cyclization process. The propargyl groups have enough chain length for flexible orientations are projected randomly in their crystal network. Their packing is

very efficient so that without having any solvent co-crystallization,2 these crystals are stable enough for diffraction studies.

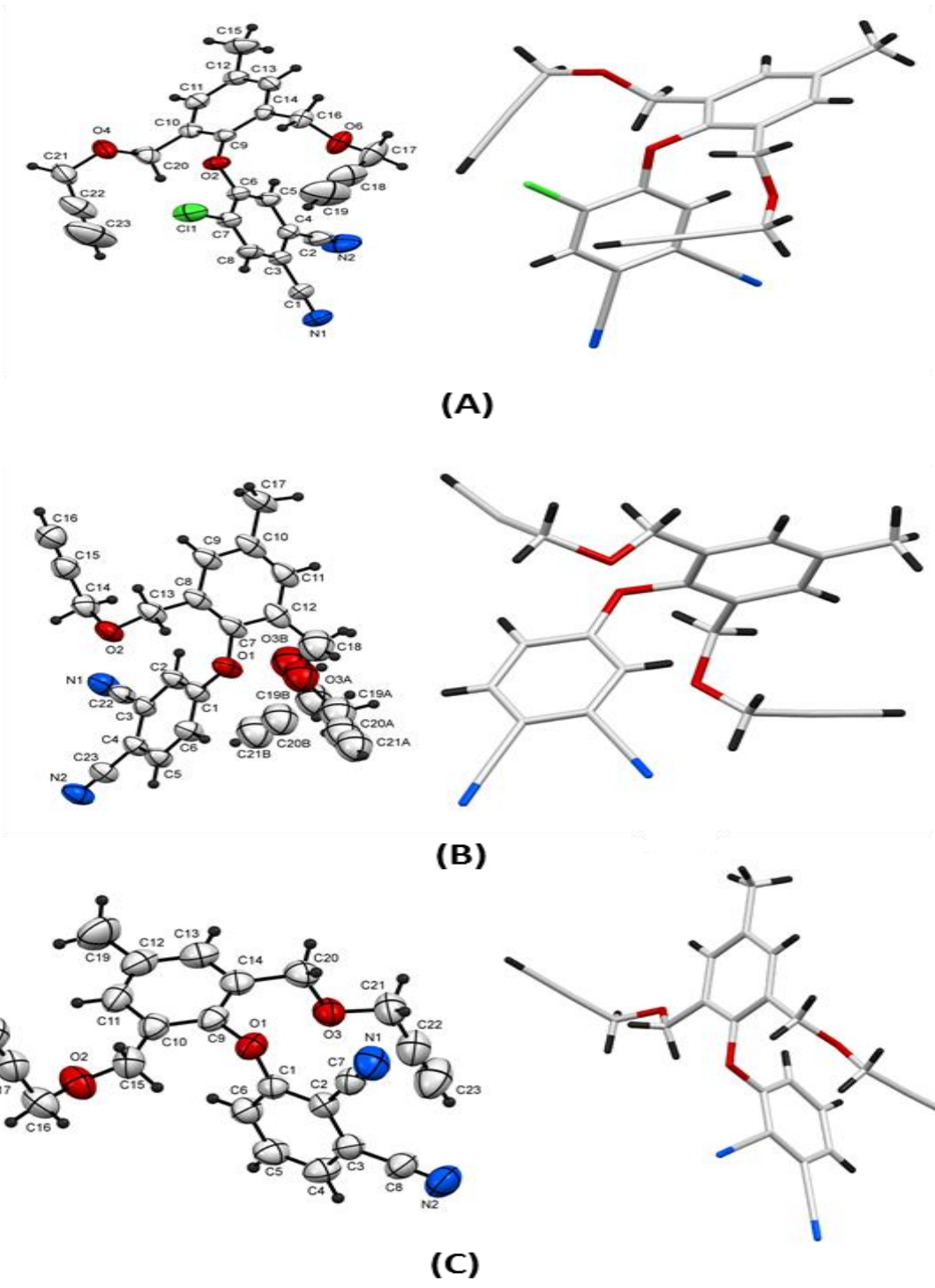

Figure S39. Crystal structure of **(A)**peripherally chlorinated Pc-precursor **4**; **(B)** peripherally substitutedPc-precursor**5** and **(C)** non-peripherally substituted Pc-precursor**6**obtained from

diffraction data thermal ellipsoid representation and capped stick representation. Color code: blue-nitrogen; gray-carbon; red-oxygen; green-chlorine and black-hydrogen.

Table S2. Summary on the nature and various crystallographic parameters of crystal samples of mono-substituted phenoxyl phthalonitriles (**4-6**).

Crystal sample	**4**	**5**	**6**
Crystal data			
Chemical formula	$C_{23}H_{17}ClN_2O_3$	$C_{46}H_{36}N_4O_6$	$C_{23}H_{18}N_2O_3$
M_r	404.84	740.79	370.41
Crystal system, space group	Monoclinic, $P2_1/c$	Triclinic, *P-1*	Triclinic, *P-1*
Temperature (K)	296	150	293
a, *b*, *c* (Å)	14.9291 (5), 10.5173 (3), 14.4180 (4)	8.4034 (9), 10.6002 (11), 12.8112 (14)	10.4756 (7), 11.1851 (8), 11.4936 (8)
β (°)	111.081 (1)	65.879 (5), 83.922 (6), 82.056 (6)	101.408 (7), 107.744 (8), 117.153 (9)
V (Å^3)	2112.31 (11)	1030.01 (19)	1047.2 (2)
Z	4	1	2
Radiation type	Cu *K*α	Mo *K*α	Mo *K*α
μ (mm^{-1})	1.81	0.08	0.08
Crystal size (mm)	0.39 × 0.29 × 0.13	0.20 × 0.16 × 0.05	0.21 × 0.20 × 0.15
Data collection			
Diffractometer	Bruker X8 Prospector	Rigaku R-AXIS RAPID	Rigaku R-AXIS RAPID
Absorption correction	Multi-scan	Multi-scan	Multi-scan
	SADABS V2008/1 (Bruker)	*ABSCOR* (Rigaku, 1995)	*ABSCOR* (Rigaku, 1995)
T_{min}, T_{max}	0.56, 0.79	0.984, 0.996	0.683, 0.988
No. of measured, independent and observed [$I > 2\sigma(I)$] reflections	19063, 3554, 3117	8066, 3608, 2152	9418, 4249, 2930
R_{int}	0.041	0.039	0.02
$(\sin\theta/\lambda)_{max}$ (Å^{-1})	0.595	0.595	0.624
Refinement			
$R[F^2 > 2\sigma(F^2)]$, $wR(F^2)$, S	0.048, 0.160, 0.86	0.106, 0.348, 1.24	0.046, 0.176, 1.14

No. of reflections	3554	3608	4249
No. of parameters	263	291	254
H-atom treatment	Independent and constrained	Constrained	Constrained
$\Delta\rho_{max}$, $\Delta\rho_{min}$ (e Å^{-3})	0.48, −0.52	0.85, −0.73	0.30, −0.19

Table S3: List of torsion angles corresponds to the phenoxyl with respect to the di-nitrile plane in **4**-**6**.

Atom list	Torsion angle	Atom list	Torsion angle
Crystal: 4			
C10-C9-O2-C6	87.99	C14-C9-O2-C6	-97.05
Crystal: 5			
C8-C7-O1-C1	91.05	C12-C7-O1-C1	-95.42
Crystal: 6			

Absorption and fluorescence spectra

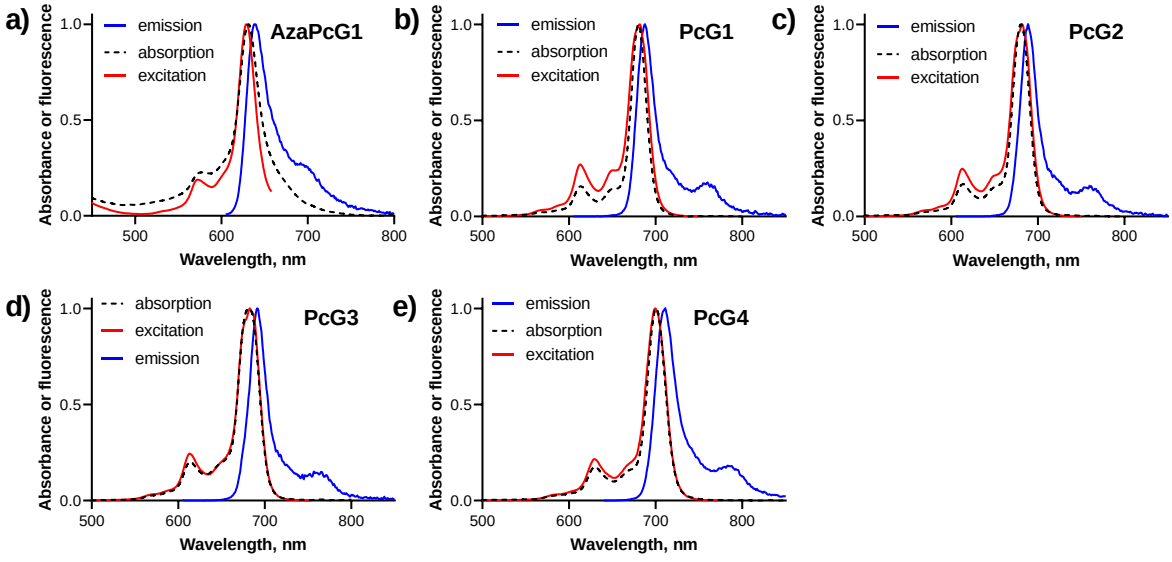

Figure S40. Normalized absorption (black, dashed), emission (blue) and excitation (red) spectra of **AzaPcG1**, **PcG1-G4** in DMF at 0.5 µM concentration at room temperature.

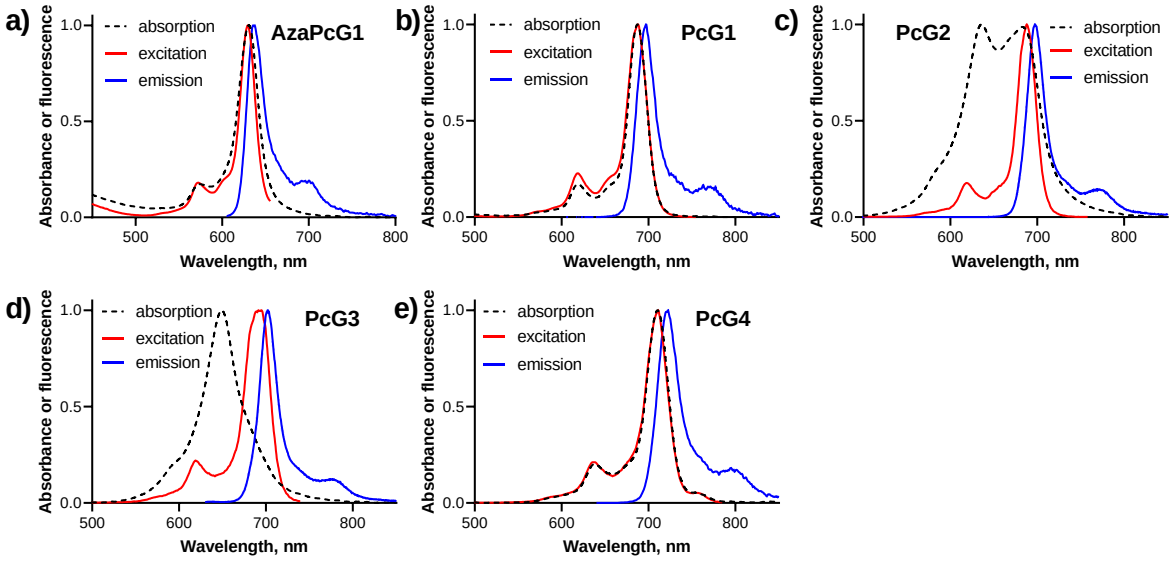

Figure S41. Normalized absorption (black, dashed), emission (blue) and excitation (red) spectra of **AzaPcG1**, **PcG1-G4** in water at 0.5 μM concentration at room temperature.

Photophysical characterization

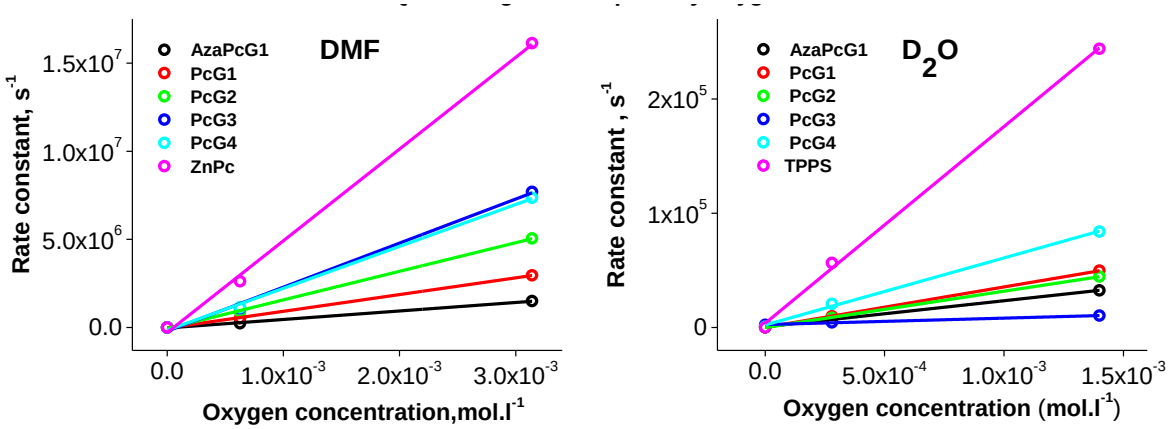

Figure S42. Stern-Volmer quenching of the triplet states by oxygen in DMF and in D_2O.

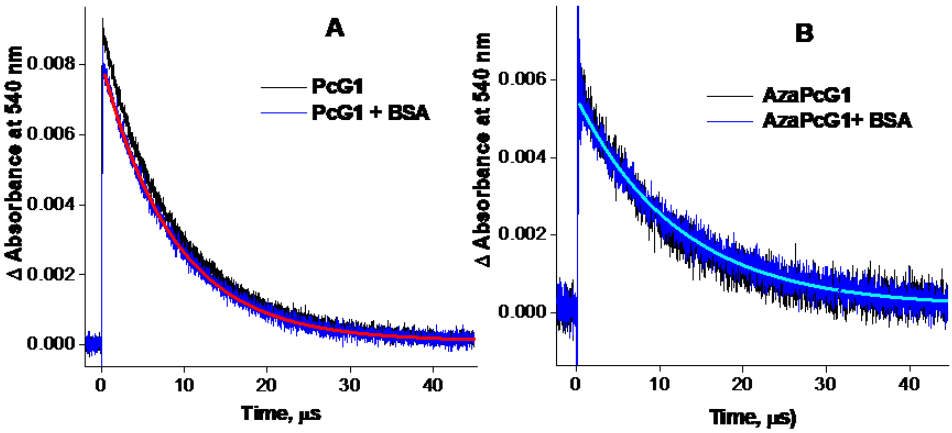

Figure S43. Influence of BSA on the triplet states kinetics of **PcG1** (panel A) and **AzaPcG1** (panel B). BSA was added to the sample in the solid state.

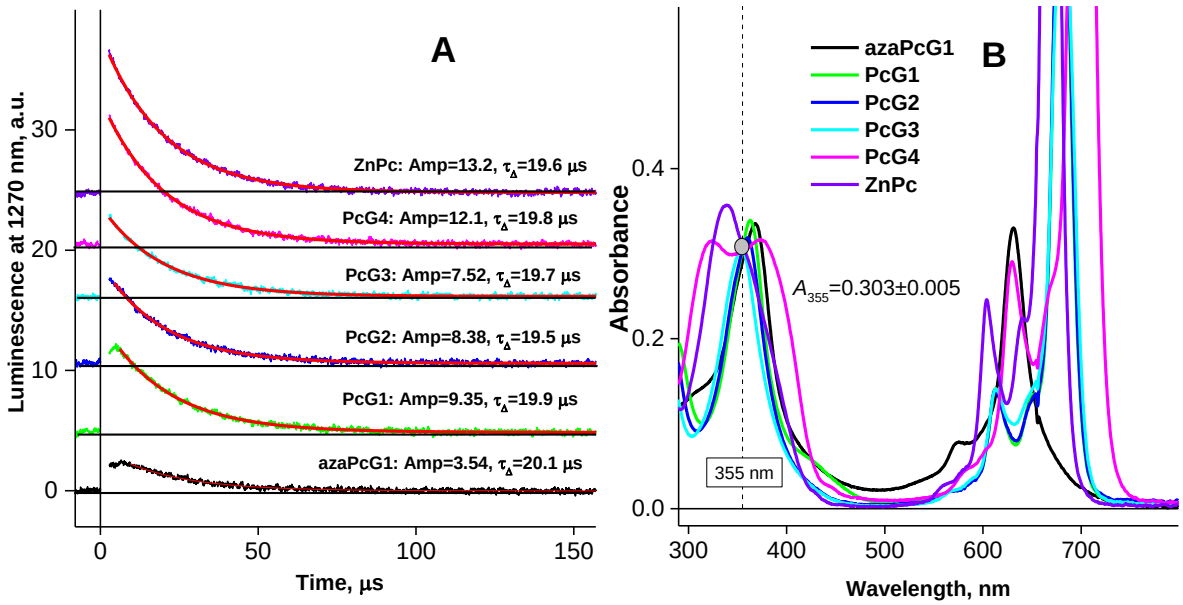

Figure S44. Panel A: Time-resolved luminescence of singlet oxygen at 1270 nm in air saturated DMF, excited by Nd-YAG laser (355 nm). Red lines are single exponential fits into experimental data; data are offset. Panel B: Corresponding UV-vis spectra.

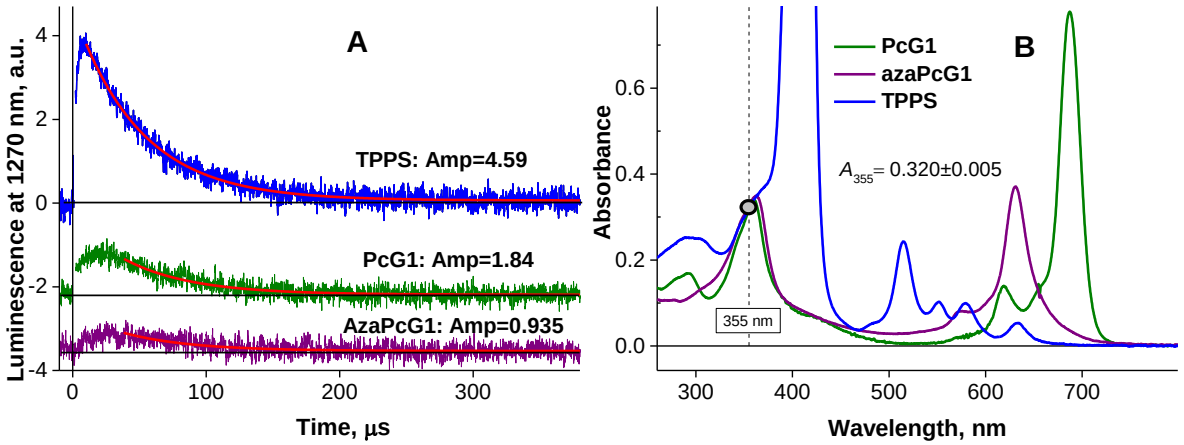

Figure S45. Panel A: Time-resolved luminescence of singlet oxygen at 1270 nm in air saturated D_2O, excited by Nd-YAG laser (355 nm). Red lines are single exponential fits into experimental data; data are offset. Panel B: Corresponding UV-vis spectra.

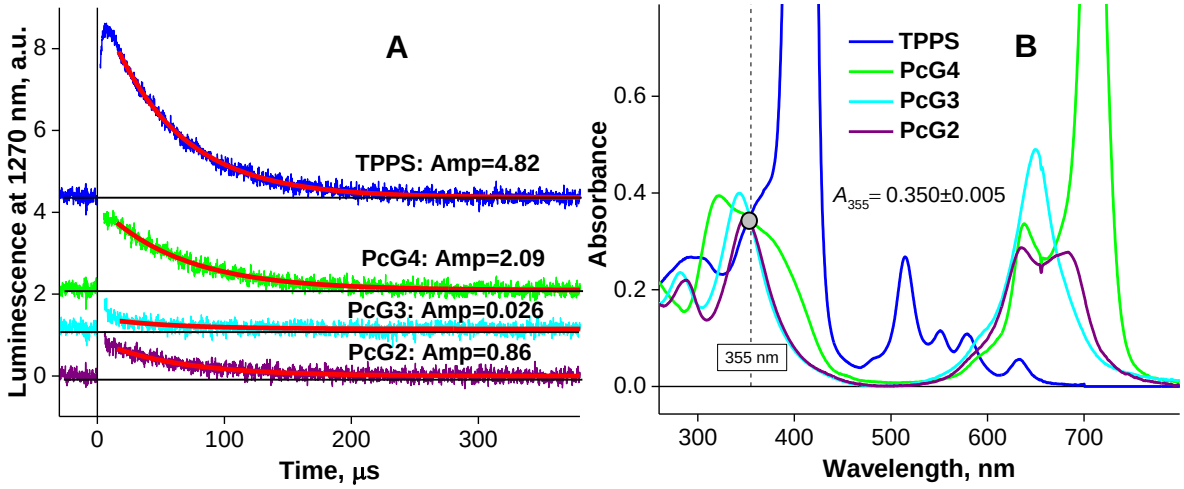

Figure S46. Panel A: Time-resolved luminescence of singlet oxygen at 1270 nm in air saturated D_2O, excited by Nd-YAG laser (355 nm). Red lines are single exponential fits into experimental data; data are offset. Panel B: Corresponding UV-vis spectra.

Paracellular transport

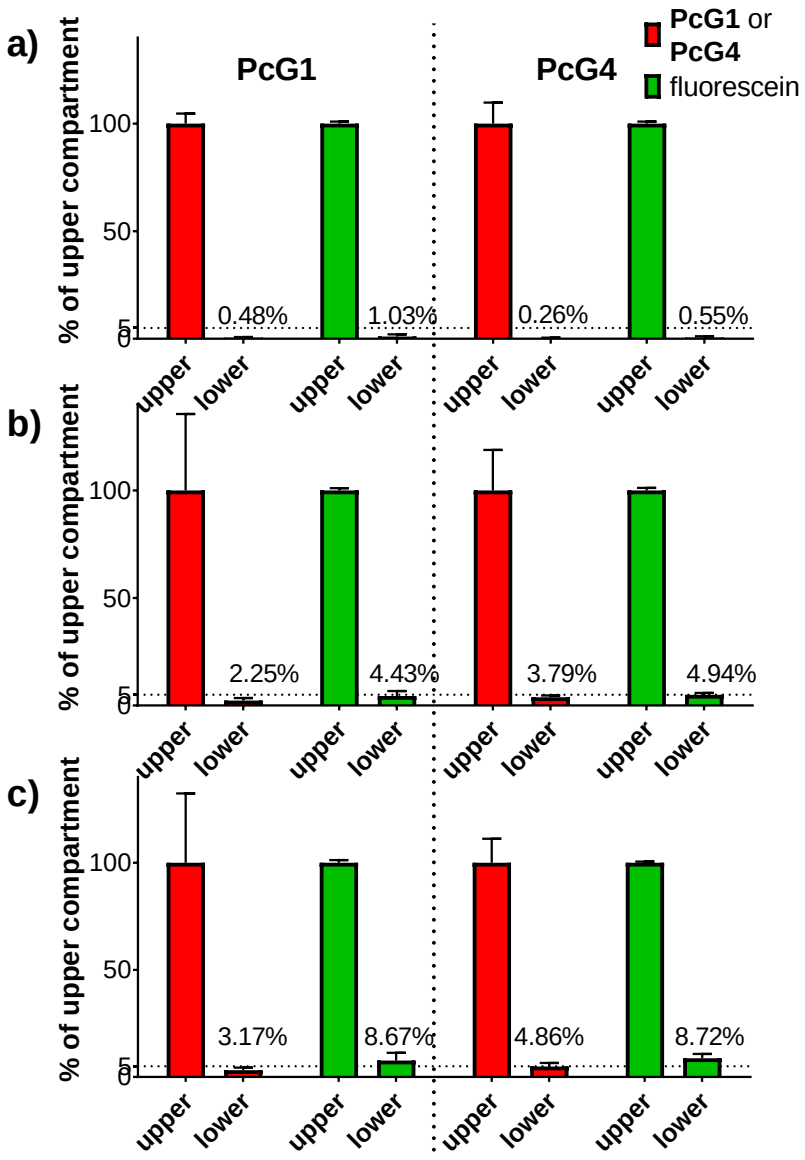

Figure S47. Assessment of paracellular transport on the layer of MDCKII cells using glycosylated Pcs (red) or fluorescein-dextran (green) just after addition of fluorescent probes (a), in 1 h (b) and in 4 h (c). The values in lower compartment are expressed related to the amount in the upper compartment which is considered 100 %.